

**A DUAL-DETECTOR OPTICAL HETERODYNE RECEIVER
FOR LOCAL OSCILLATOR NOISE SUPPRESSION**

by

GREGORY LEW ABBAS

Submitted to the Department of
Electrical Engineering and Computer Science
in Partial Fulfillment of the
Requirements for the Degrees of

**ELECTRICAL ENGINEER,
MASTER OF SCIENCE,
and
BACHELOR OF SCIENCE**

in Electrical Engineering and Computer Science

at the

Massachusetts Institute of Technology

February 1984

©Massachusetts Institute of Technology 1984

Signature of Author_____

Department of Electrical Engineering and Computer Science
January 31, 1984

Certified by_____

Vincent W. S. Chan
Thesis Supervisor

Accepted by_____

Arthur C. Smith
Chairman, Department Committee on Graduate Students

Archives

MASSACHUSETTS INSTITUTE
OF TECHNOLOGY

JUN 21 1984

LIBRARIES

**A DUAL-DETECTOR OPTICAL HETERODYNE RECEIVER
FOR LOCAL OSCILLATOR NOISE SUPPRESSION**

by

GREGORY LEW ABBAS

Submitted to the Department of
Electrical Engineering and Computer Science
on January 31, 1984 in partial fulfillment of the
requirements for the Degrees of
Electrical Engineer, Master of Science,
and Bachelor of Science
in Electrical Engineering and Computer Science

ABSTRACT

The performance of a dual-detector optical heterodyne receiver was analyzed and compared with the performance of a conventional single-detector heterodyne receiver. The dual-detector receiver is found to offer two main advantages over the single-detector receiver — (1) increased performance in the presence of local oscillator intensity fluctuations that might severely degrade single-detector receiver performance, and (2) decreased local oscillator power requirements. These two advantages are particularly important in a communication system which uses semiconductor laser diodes as local oscillators. Such lasers suffer from intrinsic wide-band intensity fluctuations and can also impose strict power constraints on receiver design.

Based on the analysis, suggestions for the optimal design of a dual-detector heterodyne receiver are made. Also, several experiments were performed to demonstrate the improved performance of the dual-detector receiver — both for unguided- and guided-wave receivers.

Thesis Supervisor: Dr. Vincent W. S. Chan

Title: Assistant Group Leader
 Communication Technology, Group 68
 M.I.T. Lincoln Laboratory

BIOGRAPHICAL NOTE

The author was born on January 14, 1961, in Grundy Center, Iowa. He lived on a farm outside of Aplington, Iowa, until graduation from high school in May, 1979. In August, 1979, he moved to Massachusetts to attend the Massachusetts Institute of Technology. He was accepted into the VI-A CO-OP program of the Department of Electrical Engineering and Computer Science at M.I.T. and has worked at the M.I.T. Lincoln Laboratory in Group 68, Communication Technology, from May, 1981, to the present. His work has dealt with analog and digital circuit design, GaAlAs semiconductor laser diode intensity noise characterization, and low-noise optical heterodyne receiver design. He has co-authored several papers [2,11,12,17,18]. He expects to receive the S.B. and S.M. degrees from M.I.T. in February, 1984, and will continue working toward his doctorate.

ACKNOWLEDGEMENTS

I would like to thank several people for the help they have given me in undertaking this thesis.

I thank my advisor, V. W. S. Chan, for his suggestion of this project and his unlimited support as the work progressed. I also thank him for pushing me to publish the results and for the help which he gave me with writing and speaking.

I thank T. K. Yee for the tremendous amount of time and help he has given me — both in the lab taking data and in writing the various papers which resulted. "Don't touch the table!"

I would also like to thank J. McHarg for his original suggestion of using a hybrid junction for subtraction and for my second Co-op assignment, F. Walther for getting me through my first Co-op assignment, W. Provencer for his help in quickly scrounging up whatever I needed to perform the experiments, A. Tidd for his ability to build hardware and keep it working, S. Howland for typing, and finally, S. Colcock, J. Roberge, J. Tucker, and L. Wereminski for the VI-A program.

TABLE OF CONTENTS

ABSTRACT	ii
BIOGRAPHICAL NOTE	iii
ACKNOWLEDGEMENTS	iv
LIST OF FIGURES	vi

<i>Chapter</i>	<i>page</i>
I. INTRODUCTION	1
II. DUAL-DETECTOR HETERODYNE DETECTION.	3
2.1 THE DUAL-DETECTOR RECEIVER MODEL	3
2.2 SNDR NEGLECTING THERMAL NOISE WITH ONE ARBITRARY GAIN	8
2.3 SNDR NEGLECTING THERMAL NOISE WITH TWO ARBITRARY ATTENUATORS	10
2.4 THE OPTIMUM BEAM SPLITTER	11
2.5 SNDR WITH THERMAL NOISE AND TWO ATTENUATORS . . .	13
2.6 SNDR WITH UNMATCHED DETECTOR FREQUENCY RESPONSES.	16
2.7 SNDR WITH UNEQUAL PATH LENGTHS	18
2.8 LOSSY BEAM SPLITTER OR COUPLER	19
III. EXPERIMENTAL RESULTS	23
3.1 UNGUIDED DUAL-DETECTOR RECEIVER	24
3.1.1 SMALL-BANDWIDTH DETECTORS	24
3.1.1.1 MATCHED PATH LENGTHS.	24
3.1.1.2 UNMATCHED PATH LENGTHS	30
3.1.2 LARGE-BANDWIDTH DETECTORS.	32
3.2 GUIDED DUAL-DETECTOR RECEIVER.	36
IV. CONCLUSIONS.	44

<i>Appendix</i>	<i>page</i>
A. COUPLER PHASE SHIFTS	46
B. SNDR BOUNDS	50
REFERENCES	54

LIST OF FIGURES

<i>Figure</i>	<i>page</i>
1. The dual-detector receiver model.	4
2. Receiver performance without thermal noise.	12
3. Receiver performance with thermal noise.	14
4. Receiver performance with and without optimum attenuators.	16
5. Constraint on a lossy coupler's phase shift.	20
6. I.F. signal degradation due to $\phi \neq 90^\circ$	21
7. Possible I.F. signal degradation vs. coupler loss.	22
8. Low-frequency experimental apparatus.	25
9. The 0° - 180° microwave hybrid junction.	26
10. Low-frequency intensity noise cancellation data (no delay).	29
11. Noise cancellation data with delay.	31
12. High-frequency experimental apparatus.	33
13. High-frequency noise cancellation data.	35
14. The measured detector frequency responses.	36
15. The single-mode fiber directional coupler.	37
16. Measurement of I.F. signal phase difference.	39
17. 80 MHz I.F. signal enhancement data.	40
18. Noise cancellation data in optical fiber.	43
19. Symmetric, linear, four-port coupler.	46

Chapter I

INTRODUCTION

The performance of a conventional single-detector optical heterodyne receiver can be severely degraded by intensity fluctuations of the receiver's local oscillator (L.O.). Such fluctuations produce at the detector photocurrent noise in excess of the usual quantum shot noise.¹ If the excess photocurrent noise is comparable to or larger than the quantum shot noise, receiver performance may be degraded. For noisy local oscillator lasers (such as semiconductor lasers), receiver performance degradation due to L.O. intensity noise can be substantial (2-40 dB) [3,4].

An optical heterodyne receiver which uses two detectors with equal quantum efficiencies has been proposed by several authors [5,6,7,8,9]. Such a receiver uses its two detectors in a balanced-mixer configuration to suppress the photocurrent noise resulting from local oscillator intensity fluctuations. More recently, the receiver model has been generalized to include unmatched detector quantum efficiencies and an arbitrary gain applied to one of the detector outputs [10,11]. This arbitrary gain is used to correct for unbalanced noise signals and to improve the overall receiver signal-to-noise ratio.

In this thesis, the local oscillator noise cancellation properties of such dual-detector receivers will be discussed. The work will also include a discussion of several other parameters that affect dual-detector receiver design and performance, including amplifier thermal noise, non-flat or unmatched detector frequency responses, unequal

¹ Photocurrent noise produced by local oscillator intensity fluctuations will be referred to as being "excess noise" or "local oscillator noise." Photocurrent noise due to the quantum detection process will be called "shot noise."

optical or electrical path lengths in the two branches of the receiver, and lossy beam splitters or couplers [2]. These effects put constraints on the design of a practical receiver. Suggestions for building an optimum dual-detector heterodyne receiver will be given. The results of several experiments which demonstrate local oscillator noise cancellation will be presented, both for unguided- and guided-wave dual-detector optical heterodyne receivers.

Chapter II

DUAL-DETECTOR HETERODYNE DETECTION

In this chapter, a model for the dual-detector local-oscillator-intensity-noise-cancellation receiver is presented and analyzed. By scaling the photocurrents produced in the two detectors and subtracting, nearly quantum limited performance is attainable, even in the presence of large local oscillator intensity fluctuations. The optimum beam splitter is found, and the dual-detector receiver performance is compared with that of the conventional single-detector receiver. It is shown that the presence of amplifier thermal noise in the receiver can have an effect on the optimum choices of beam splitter and scaling factors. Unmatched detector frequency responses can degrade dual-detector receiver performance significantly. The effect of unequal signal path lengths in the two branches of the receiver is described. The final section of the analysis deals with the difficulties which arise when the beam splitter or coupler used to combine the local oscillator and received signal beams is lossy.

2.1 THE DUAL-DETECTOR RECEIVER MODEL

An optical dual-detector heterodyne receiver uses a beam splitter to combine a weak received signal beam (average power S^1) with a stronger local oscillator beam (average power L^1). S and L are assumed to be real. (See figure 1.) Normally, the two beams are aligned in polarization so that the fields add. The inputs to the beam splitter are the received signal field $S = \sqrt{2} \cdot S \cdot e^{j\omega_1 t}$ and the local oscillator field $L = \sqrt{2} \cdot L \cdot e^{j\omega_2 t}$. If the beam splitter is linear, lossless,¹ and symmetric, the output fields

¹ Lossy beam splitters (and couplers) are considered in Section 2.8.

E_1 and E_2 are obtained by the transformation:

$$\begin{bmatrix} E_1 \\ E_2 \end{bmatrix} = e^{j\phi_r} \begin{bmatrix} \sqrt{1-\epsilon} & \sqrt{\epsilon} e^{j\pi/2} \\ \sqrt{\epsilon} e^{j\pi/2} & \sqrt{1-\epsilon} \end{bmatrix} \begin{bmatrix} S \\ L \end{bmatrix} \quad (1)$$

where ϵ and $1-\epsilon$ are the power transmission and reflection coefficients, respectively, of the beam splitter and ϕ_r is the phase shift of the reflected field. (See Appendix A.)

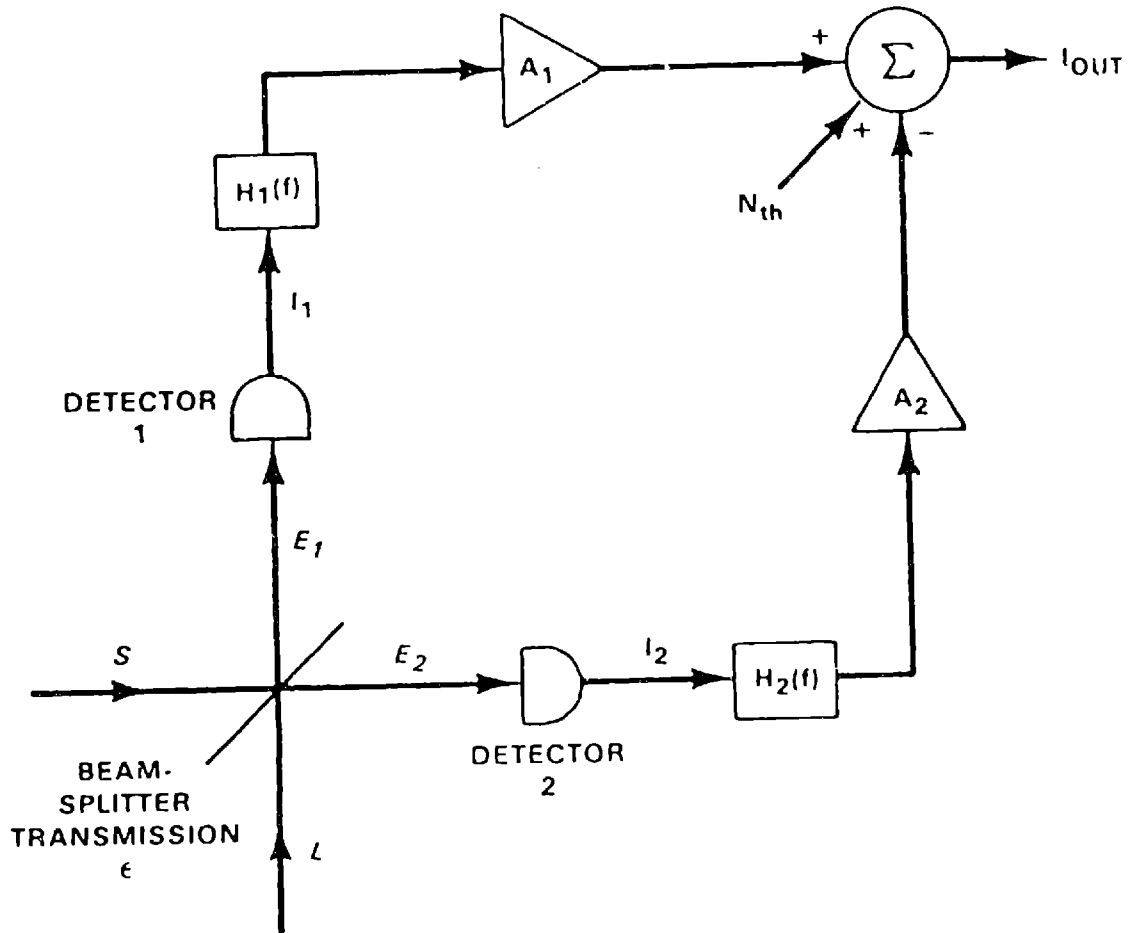


Figure 1: The dual-detector receiver model.

The photocurrents produced in the detectors are conditional Poisson processes. After filtering, the photocurrent in each detector is a Gaussian process with mean proportional to the power of the impinging optical field and a spectral height which can be determined [12]. If the quantum efficiencies of the two detectors are η_1 and η_2 , respectively, the means of the photocurrents I_1 and I_2 are:

$$\begin{aligned}\bar{I}_1 &= \frac{\eta_1 e}{h\nu} \frac{1}{2} |\mathcal{E}_1|^2 \\ &= \frac{\eta_1 e}{h\nu} \{ (1-\epsilon)S^2 + \epsilon L^2 + 2SL\sqrt{\epsilon(1-\epsilon)} \cdot \cos[(\omega_1 - \omega_2)t + \phi_1 - \phi_2 - \pi/2] \}\end{aligned}\quad (2)$$

$$\begin{aligned}\bar{I}_2 &= \frac{\eta_2 e}{h\nu} \frac{1}{2} |\mathcal{E}_2|^2 \\ &= \frac{\eta_2 e}{h\nu} \{ \epsilon S^2 + (1-\epsilon)L^2 + 2SL\sqrt{\epsilon(1-\epsilon)} \cdot \cos[(\omega_1 - \omega_2)t + \phi_1 - \phi_2 - \pi/2] \}\end{aligned}\quad (3)$$

The mean photocurrents contain a D.C. component and a component at the I.F. difference frequency $(\omega_1 - \omega_2)$ of the signal and local oscillator fields. If:

$$\frac{L^2}{S^2} \gg \text{MAX}\left(\frac{1-\epsilon}{\epsilon}, \frac{\epsilon}{1-\epsilon}\right) \quad (4)$$

the S^2 term in each photocurrent can be neglected.

The zero-mean Gaussian noise components of the photocurrents will have one-sided spectral density $2eI + 2e\gamma(f)I^2$. The first term is the white quantum shot noise generated in a photodetector with D.C. photocurrent I . The second term is due to the intensity fluctuations of the local oscillator. The local oscillator noise density has been found to vary as D.C. photocurrent squared and can be quantified by the param-

eter γ .³ Thus, the noise power densities, N_1 and N_2 , for the two detectors can be written:

$$N_1 = 2eI_{1,DC} + 2e\gamma I_{1,DC}^2 \quad (5)$$

$$N_2 = 2eI_{2,DC} + 2e\gamma I_{2,DC}^2 \quad (6)$$

Equations 2 and 3 show that the I.F. components of the two photocurrents must be 180° out of phase. However, by the assumption of relatively large local oscillator power, the excess noise generated at the two detectors is due mainly to L.O. intensity fluctuations which reach both detectors simultaneously.⁴ Therefore, the excess noise in the two detectors will be in phase, though not necessarily equal in magnitude. By *subtracting* the two detectors' photocurrents, it should be possible to increase the I.F. signal power while decreasing the excess noise power. The resulting local-oscillator noise suppression is similar to that obtained in a microwave balanced mixer [1].

The two shaping filters, $H_1(f)$ and $H_2(f)$, are included in the dual-detector receiver model to account for possibly unequal detector frequency responses. For now, it will be assumed that $H_1(f)=H_2(f)=1$. Also, two arbitrary noiseless amplifiers (or atten-

³ γ has units of inverse current. Typical values of γ range from 10^2 to 10^3 A⁻¹ depending on frequency and output power for GaAlAs semiconductor lasers [18]. A value of $\gamma=10^3$ A⁻¹ would imply that the photocurrent noise density produced in a detector with 1 mA of D.C. photocurrent was 3 dB above the quantum shot noise density.

⁴ The effect of unequal optical path lengths is discussed in Section 2.7.

uators) with current gains A_1 and A_2 have been inserted. The gains of these amplifiers can be adjusted to optimize the overall receiver's signal-to-noise-density ratio. A variable level of thermal noise, N_{th} , has also been added to the receiver model.⁵ For now, it will be assumed that the receiver thermal noise is negligible compared to the quantum shot noise⁶ so that $N_{th}=0$. With $N_{th}=0$, the amplifiers A_1 and A_2 are redundant. Thus, let $A_2=1$ and only vary A_1 .

After the scaling amplifier A_1 , the I.F. photocurrent and photocurrent noise power terms are equal to $A_1 I_1$ and $A_1^2 N_1$. Subtracting I_2 and N_2 gives the dual-detector I.F. beat signal (I_-) and noise power (N_-) terms:

$$\bar{I}_- = 2 \frac{e}{\hbar \omega} \sqrt{\epsilon(1-\epsilon)} S L (A_1 \eta_1 + \eta_2) \cdot \cos[(\omega_1 - \omega_2)t + \phi_1 - \phi_2 - \pi/2] \quad (7)$$

$$N_- = 2e(A_1^2 I_{1,DC} + I_{2,DC}) + 2e\gamma(A_1 I_{1,DC} - I_{2,DC})^2 \quad (8)$$

The signal-to-noise-density ratio, SNDR, is therefore:

$$SNDR_- = \frac{\epsilon(1-\epsilon)(A_1 \eta_1 + \eta_2)^2 S^2 / \hbar \omega}{A_1^2 \epsilon \eta_1 + (1-\epsilon)\eta_2 + \frac{e}{\hbar \omega} L^2 [A_1 \eta_1 \epsilon - \eta_2(1-\epsilon)]^2} \quad (9)$$

⁵ As a first approximation, the thermal noise has been inserted after the adjustable gains and is assumed to be independent of the magnitudes of the gains. A more realistic model would have N_{th} being a function of the scaling gains, but this would unnecessarily complicate the model at this point.

⁶ Section 2.5 deals with the problem of nonnegligible thermal noise.

To derive the SNDR of detector 1 or 2 separately, just let A_1 go to ∞ or 0, respectively. Thus, for detector 1, the SNDR is:

$$\text{SNDR}_1 = \frac{(1-\epsilon)\eta_1 s^2/\kappa\omega}{1 + \frac{eY_L^2}{\kappa\omega}\eta_1\epsilon} \quad (10)$$

Similarly, for detector 2:

$$\text{SNDR}_2 = \frac{\epsilon\eta_2 s^2/\kappa\omega}{1 + \frac{eY_L^2}{\kappa\omega}\eta_2(1-\epsilon)} \quad (11)$$

Since the single-detector receiver is a special case of the dual-detector receiver and is not necessarily optimum, it is clear that the dual-detector receiver must always perform at least as well as the single-detector receiver.

2.2 SNDR NEGLECTING THERMAL NOISE WITH ONE ARBITRARY GAIN

When Eq. 9 is maximized over A_1 , an optimum gain is found:

$$A_{1,\text{OPT}} = \frac{1-\epsilon}{\epsilon} \cdot \frac{1+\eta_2\beta}{1+\eta_1\beta} \quad (12)$$

where $\beta = \frac{eY_L^2}{\kappa\omega}$.

Substituting the value of $A_{1,\text{OPT}}$ back into Eq. 9 yields:

$$\text{SNDR} = \frac{[(1+\eta_2\beta)(1-\epsilon)\eta_1 + (1+\eta_1\beta)\epsilon\eta_2]^2 s^2/\kappa\omega}{(1+\eta_2\beta)^2(1-\epsilon)\eta_1 + (1+\eta_1\beta)^2\epsilon\eta_2 + \beta(\eta_1-\eta_2)^2\epsilon(1-\epsilon)} \quad (13)$$

For the case of $\eta_1 = \eta_2 = \eta$, $A_{1,OPT} = (1-\epsilon)/\epsilon$ which depends only on the beam splitter transmission ϵ and not on the excess noise parameter γ . Thus, for matched detectors the optimum receiver can be designed without prior knowledge of the local oscillator excess noise characteristics. The excess noise term in the denominator goes to zero and the SNDR is the same as for a single-detector heterodyne receiver (Eq. 10) with quantum efficiency η , no local oscillator intensity noise, and $\epsilon=0$. However, the local oscillator power required for the single-detector receiver is much larger since ϵ is close to 0 and most of the L.O. power is wasted. For the dual-detector receiver with $\eta_1 = \eta_2$, ϵ can be set equal to 1/2 and the same SNDR is achieved with much less local oscillator power.

If $\eta_1 \neq \eta_2$, the excess noise will not be canceled completely when $A_{1,OPT}$ is used (except for the case $\gamma \rightarrow \infty$). For semiconductor laser local oscillators with typical γ (around 10^{-3} A^{-1} at 100 MHz) and for $\epsilon=1/2$, the excess noise will be reduced by a factor of $(\eta_1 - \eta_2)^2$. In fact, it can be shown (see Appendix B) that with the optimum gain, the dual-detector SNDR expression is bounded:

$$\frac{S}{\hbar\omega} \cdot \text{MIN}(\eta_1, \eta_2) < \text{SNDR} < \frac{S}{\hbar\omega} \cdot \text{MAX}(\eta_1, \eta_2) \quad (14)$$

This bound holds for all beam splitters (ϵ) and excess noise levels (γ), even as $\gamma \rightarrow \infty$.

Even if the two detectors' quantum efficiencies are not well-matched, the performance of the dual-detector receiver *with optimizing gain* is rather insensitive to the excess noise level. This is important since it implies that receiver performance will not degrade substantially if for some reason the local oscillator becomes noisier (e.g. due

to aging). However, since $A_{1,OPT}$ does depend on γ when $\eta_1 \neq \eta_2$ and γ is in general a function of frequency, $A_{1,OPT}$ will be a function of frequency. This property is undesirable, so it is important to keep the detectors well-matched.

Notice, also, that the performance bound does not depend on ϵ . Thus, the beam splitter may be chosen based on other factors — namely L.O. power and thermal noise. This independence of performance on ϵ assumes, of course, that it is possible to implement $A_{1,OPT}$.

2.3 SNDR NEGLECTING THERMAL NOISE WITH TWO ARBITRARY ATTENUATORS

A dual-detector receiver with an arbitrarily large gain and no thermal noise is not very realistic. A more realistic model to consider is one which constrains A_1 and A_2 to be arbitrary noiseless attenuators with magnitudes between 0 and 1. For the receiver with no thermal noise, the two models are equivalent. However, when the effect of thermal noise is discussed in Section 2.5, limiting the receiver model to two attenuators will produce more realistic results. Thus, the SNDR calculations must be modified to include two arbitrary, noiseless attenuators. With this change, the SNDR becomes:

$$SNDR_{-} = \frac{\epsilon(1-\epsilon)(A_1\eta_1 + A_2\eta_2)^2 S^2 / \kappa\omega}{A_1^2\epsilon\eta_1 + A_2^2(1-\epsilon)\eta_2 + \beta[A_1\eta_1\epsilon - A_2\eta_2(1-\epsilon)]} \quad (15)$$

The optimum attenuator values follow directly from the previous optimum gain calculation if the magnitude of at least one of the attenuators is equal to 1, i.e. no attenuation in at least one of the signal paths. Later, when non-negligible thermal noise is added to the receiver model, this condition will be optimum. Thus:

$$\Lambda_{1,OPT} = \min \left(1, \frac{1-\epsilon}{\epsilon} \cdot \frac{1+\eta_2\beta}{1+\eta_1\beta} \right) \quad (16)$$

$$\Lambda_{2,OPT} = \min \left(1, \frac{\epsilon}{1-\epsilon} \cdot \frac{1+\eta_1\beta}{1+\eta_2\beta} \right) \quad (17)$$

2.4 THE OPTIMUM BEAM SPLITTER

A second parameter which can be varied to optimize the receiver SNDR is the transmission coefficient ϵ of the beam splitter. Figure 2 shows the SNDR for both a single-detector receiver (dashed line) and two dual-detector receivers (solid lines) as ϵ is varied. 0 dB is defined to be the SNDR of a single-detector receiver (detector 1) with $\eta_1=1$, no thermal noise, no excess noise, and ϵ approaching 0. As stated in Section 2.1, the SNDR of the dual-detector receiver is always greater than or equal to the SNDR of the single-detector receiver.

If the two detectors have equal quantum efficiencies (upper solid line), all values of ϵ will give equal performance with the optimum attenuators. This is the same result that was obtained earlier with Eq. 13.

However, if $\eta_1 > \eta_2$ (lower solid line), then the optimum ϵ (ϵ_{OPT}) is 0. Intuitively, both the I.F. signal power and the quantum noise power in detector 1 are decreasing as ϵ , while the excess noise level decreases as ϵ^2 . Since the model neglects thermal noise, a small signal level does not hurt the theoretical receiver performance as long as the noise level is also small. Letting $\epsilon \rightarrow 0$ optimizes the ratio. Also, as $\epsilon \rightarrow 0$, the opti-

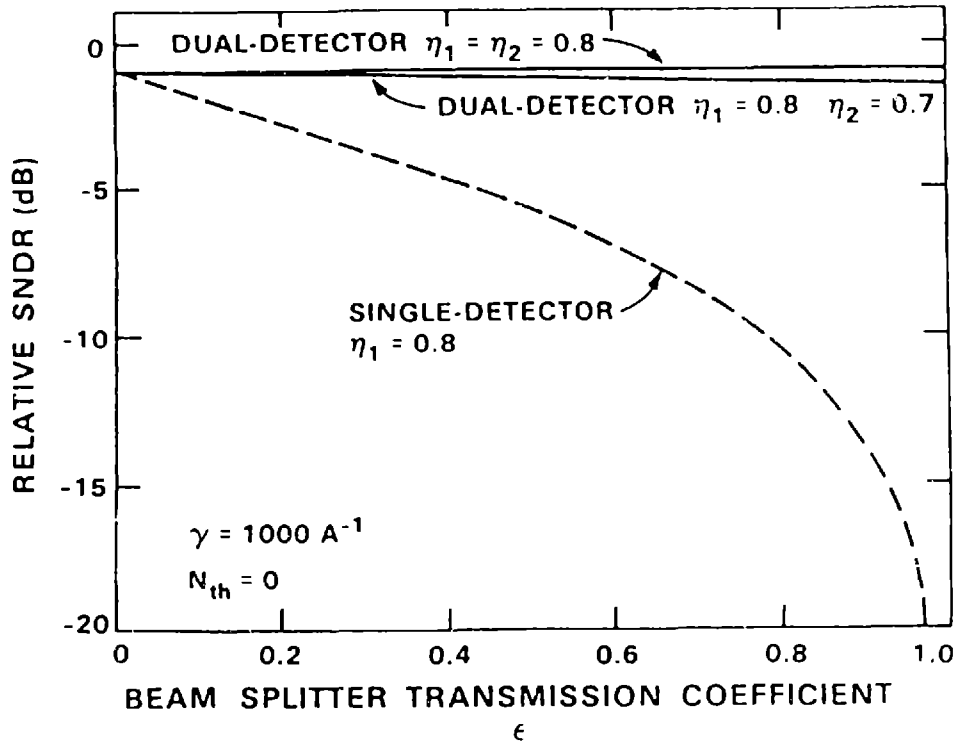


Figure 2: Receiver performance without thermal noise.

imum attenuator values go to $A_{1,OPT}=1$ and $A_{2,OPT}=0$. Thus, the receiver is effectively a single-detector receiver using only detector 1. Similarly, if $\eta_1 < \eta_2$, then $\epsilon_{OPT}=1$, $A_{1,OPT}=0$ and $A_{2,OPT}=1$. (Unfortunately for both cases, the L.O. power must increase to infinity.) With no thermal noise and unmatched detectors, the optimum dual-detector receiver makes use of the detector with higher quantum efficiency only, and a single-detector receiver performs equally well provided there is sufficient local oscillator power available. Of course, the dual-detector receiver signal-to-noise ratio would not be significantly degraded if the two detectors were nearly matched and ϵ was chosen to be 1/2 to save local oscillator power.

2.5 SNDR WITH THERMAL NOISE AND TWO ATTENUATORS

The real advantage of the dual-detector receiver over the single-detector receiver appears when there is non-negligible thermal noise in the receiver. Figure 3 shows the SNDR with thermal noise for both a single-detector receiver (dashed line) and a dual-detector receiver (solid line).⁷ The optimum ϵ is constrained away from the extreme values of 0 and 1. This is due to the fact that as ϵ approaches 0 or 1, the I.F. signal power (which goes as $\epsilon(1-\epsilon)$) becomes very small, whereas the total noise is lower bounded by the fixed thermal noise and therefore the SNDR decreases. Since the choice of beam splitter is now constrained away from the extreme values of ϵ , local oscillator intensity fluctuations can degrade the single-detector receiver performance and the dual-detector receiver can yield a significant improvement.

Adding thermal noise, N_{th} , to Eq. 13 yields:

$$SNDR_{-} = \frac{2\left(\frac{e}{h\nu}\right)^2 \epsilon(1-\epsilon) S^2 L^2 (A_1 \eta_1 + A_2 \eta_2)^2}{2e(A_1^2 I_1 + A_2^2 I_2) + 2e\gamma(A_1 I_1 - A_2 I_2)^2 + N_{th}} \quad (18)$$

where I_1 and I_2 are the D.C. components of the two detectors' photocurrents.

⁷ The thermal noise level has been set to 1/4 the quantum shot noise level of the dual-detector receiver, which is typical of a receiver using a 50 Ω front-end amplifier with 1 mA of D.C. photocurrent. Also, a fixed local oscillator power was used, since otherwise the L.O. power could be continually increased until the thermal noise again became negligible compared to the quantum shot noise.

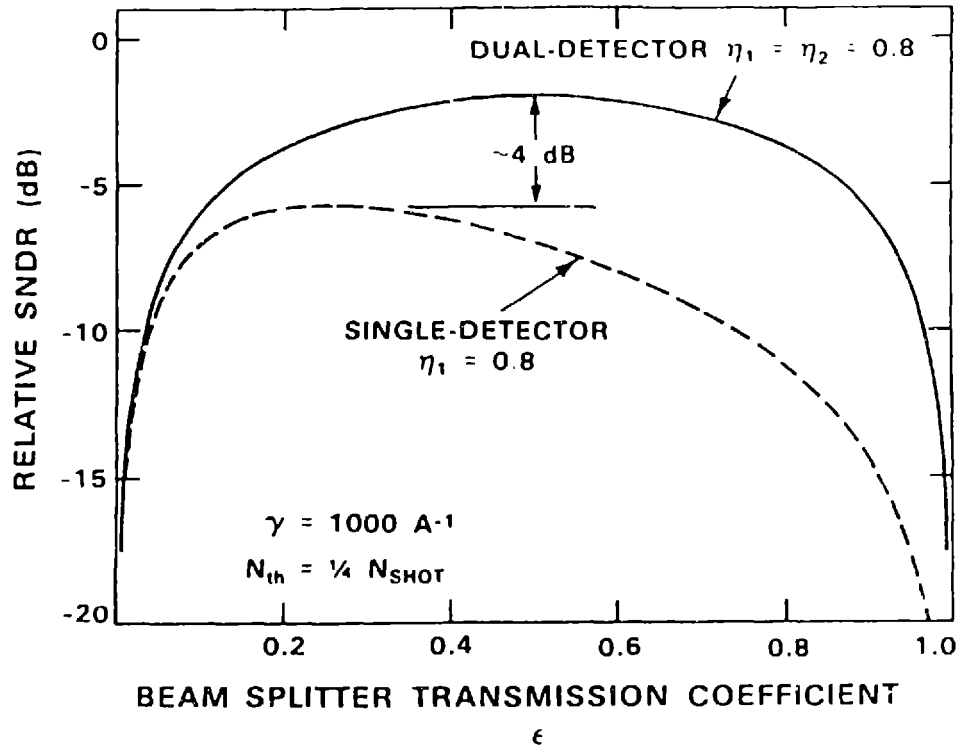


Figure 3: Receiver performance with thermal noise.

The new values for the SNDR optimizing attenuators are:

$$\Lambda_{1,OPT} = \text{MIN} \left\{ 1, \frac{(1-\epsilon)(1+\eta_2\beta) + N_{th} \cdot \frac{\hbar\omega}{2e^2\eta_2L^2}}{\epsilon(1+\eta_1\beta)} \right\} \quad (19)$$

$$\Lambda_{2,OPT} = \text{MIN} \left\{ 1, \frac{\epsilon(1+\eta_1\beta) + N_{th} \cdot \frac{\hbar\omega}{2e^2\eta_1L^2}}{(1-\epsilon)(1+\eta_2\beta)} \right\} \quad (20)$$

The presence of thermal noise always increases the magnitude of the optimum attenuators (if they are not already equal to one). Even for $\eta_1=\eta_2$, the excess noise will not in general be canceled as it was for the receiver without thermal noise. Intuitively, the optimum receiver sacrifices some amount of excess noise cancellation in order to increase the absolute I.F. signal level of one detector with respect to the thermal noise level.

When $\eta_1=\eta_2$, the value of ϵ is $1/2$ independent of the excess noise level (γ) or the thermal noise level (N_{th}). This is because of the $\epsilon(1-\epsilon)$ dependence of the I.F. signal power. However, the width of the SNDR maximum around $\epsilon_{OPT}=1/2$ (i.e., the range of ϵ for which good cancellation is possible) does depend on γ and N_{th} .

Interestingly, if $\eta_1=\eta_2$ there is a range of values of ϵ around $1/2$ where the optimum attenuators for the dual-detector receiver with thermal noise are $A_{1,OPT}=A_{2,OPT}=1$. For this range of ϵ , no attenuators are needed, simplifying the receiver design. As the thermal noise increases with respect to the quantum shot noise of the receiver, the range of ϵ for which this effect occurs increases. Figure 4 shows the difference between the SNDR for a dual-detector receiver which uses optimum attenuators and the SNDR for one which holds $A_1=A_2=1$ (i.e. no attenuators). For semiconductor laser local oscillators with $\gamma=10^3 \text{ A}^{-1}$ representing a relatively quiet L.O. (solid lines), there is little difference in performance between the two receivers for $0.4 < \epsilon < 0.6$. However, if γ increases to 10^5 A^{-1} representing a fairly noisy L.O. (dashed lines), the need for either the optimum attenuators or a tight constraint on ϵ becomes apparent. As previously noted (Section 2.2), the dual-detector receiver's performance is relatively insensitive to the excess noise level when the optimum attenuators are used.

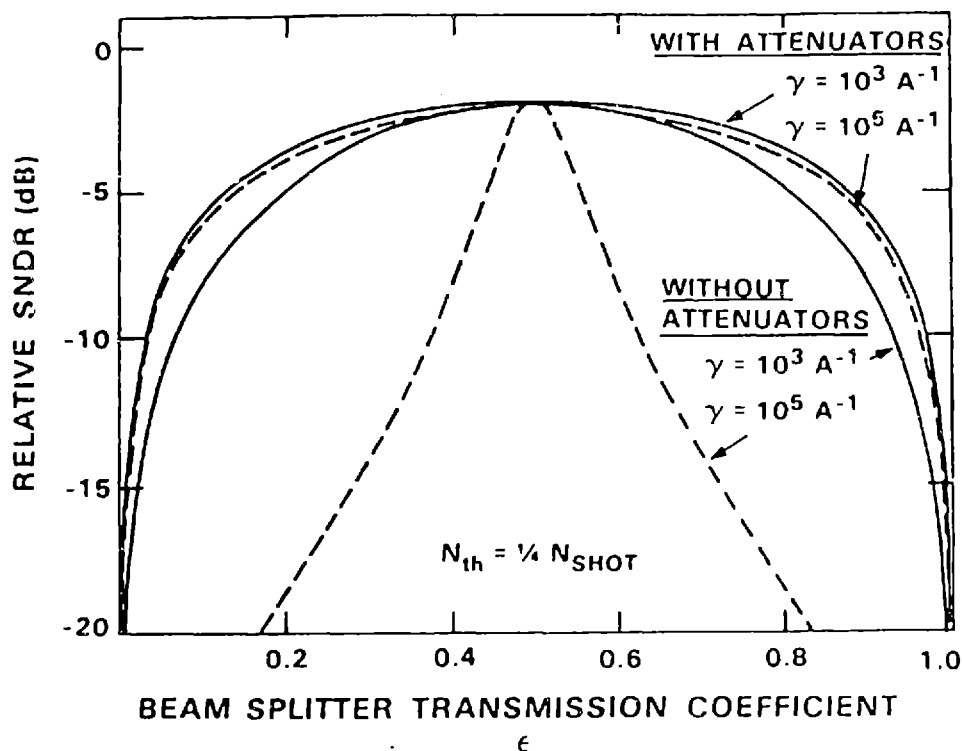


Figure 4: Receiver performance with and without optimum attenuators.

2.6 SNDR WITH UNMATCHED DETECTOR FREQUENCY RESPONSES

A further difficulty that may degrade the performance of a dual-detector receiver occurs when the two detectors have differing frequency responses. This problem could arise, for example, if the detectors have different bandwidths. For good cancellation, the L.O. noise photocurrents in both detectors must be well-matched both in amplitude and phase over the entire frequency band of interest. If one detector begins to roll off before the other near the edge of the frequency band, poor cancellation could result. For 20 dB of cancellation with a 50/50 beam splitter and both attenuators equal to 1, the detector responses must be matched within at least 1.6 dB (assuming

matched phases) and 11° (assuming matched amplitudes). Clearly, if one detector has not only rolled off by 3 dB but also acquired a 45° phase shift, poor cancellation will result.

Unmatched detector frequency responses can also occur because of line resonances in the two signal paths when the detectors are physically connected into a circuit. The detectors look like a large resistance (MΩ) in parallel with a small capacitance (pF). This makes them difficult to match to a 50Ω line and thus line resonances can result. If the noise in each detector is unequally amplified due to differing line resonances in the two signal paths, the balanced-mixer action of the dual-detector receiver may be disrupted.⁸ In fact, an attenuator designed to maximize the SNDR of a particular receiver might change the line resonances of the signal path in which it is placed enough to lower the overall SNDR rather than increase it as predicted.

If the complex frequency responses of the two branches of the dual-detector receiver are modelled as the shaping filters, $H_1(f)$ and $H_2(f)$, the output of the receiver after subtraction is:

$$\text{SNDR}_{-} = \frac{2\left(\frac{e}{4\pi\omega}\right)^2 \epsilon(1-\epsilon) S^2 L^2 |A_1 \eta_1 H_1(f_{IF}) + A_2 \eta_2 H_2(f_{IF})|^2}{2\epsilon [A_1^2 I_1 |H_1(f)|^2 + A_2^2 I_2 |H_2(f)|^2] + 2e\gamma |A_1 I_1 H_1(f) - A_2 I_2 H_2(f)|^2} \quad (21)$$

where:

$$f_{IF} = \frac{\omega_1 - \omega_2}{2\pi} \quad (22)$$

⁸ This difficulty was encountered in the experiments. See Section 3.1.2.

The magnitudes-squared of the frequency responses, $|H_1(f)|^2$ and $|H_2(f)|^2$, can be measured with an incoherent white light source to obtain an upper bound on receiver performance:

$$\text{SNDR} \leq \frac{2 \left(\frac{e}{h\nu} \right)^2 \epsilon (1-\epsilon) S^2 L^2 \{ \Lambda_1 \eta_1 |H_1(f_{IF})| + \Lambda_2 \eta_2 |H_2(f_{IF})| \}^2}{2e \{ \Lambda_1^2 I_1 |H_1(f)|^2 + \Lambda_2^2 I_2 |H_2(f)|^2 \} + 2e\gamma \{ \Lambda_1 I_1 |H_1(f)| - \Lambda_2 I_2 |H_2(f)| \}^2} \quad (23)$$

This bound holds with equality for all f where the two frequency responses are in phase.

The degradation due to line resonances can be minimized by keeping the two electrical path lengths as short as possible to push any line resonances out to frequencies higher than those of interest. This problem with implementing the optimum attenuators is another reason why it is desirable to use well-matched detectors and a beam splitter with $\epsilon=1/2$. Then no attenuators are necessary for optimum performance.

2.7 SNDR WITH UNEQUAL PATH LENGTHS

Excess noise cancellation can be degraded by unequal optical or electrical signal path lengths in the two branches of the dual-detector receiver. A differential delay T , either optical or electrical, between the beam splitter and the photocurrent subtraction point gives a relative phase shift to one branch of the receiver. This phase shift is linear with frequency. The relative phase shift between the I.F. signals due to the optical delay will be $(\omega_1 - \omega_2)T \cdot 360 / (2\pi)$ degrees. The excess noise components in the two detectors will also be given a relative phase shift equal to $f \cdot T \cdot 360$ degrees. In general, the excess noise will not be well canceled when the two photocurrents are subtracted. The problem can, of course, be corrected by simply inserting an equal delay, either optical or electrical, in the opposite signal path.

At frequency f , the differential time delay T , necessary to give a θ degree phase shift is:

$$T = \frac{\theta}{360^\circ} \cdot \frac{1}{f} \quad (24)$$

A reasonable limit to the allowable differential phase shift between the two branches of the receiver is around 11° (see Section 2.6). This phase shift will still yield a 20 dB reduction in the excess noise if all other parameters are optimum. For θ equal to 11° and $f=1$ GHz, T is ~ 30 picoseconds which corresponds to an optical path difference of ~ 9 millimeters or an electrical path difference of a few millimeters. Differential path lengths significantly greater than these limits may disrupt excess noise cancellation at high frequencies.

2.8 LOSSY BEAM SPLITTER OR COUPLER

Until now it has been assumed that the beam splitter used to couple the received signal beam with the local oscillator beam was lossless. This condition gives rise to the 90° phase shift between each input field's two outputs (see Appendix A). The 90° phase shift in turn leads to the 180° I.F. signal phase shift and enhancement as described in Section 2.1.

If the device used to couple the two fields is lossy, the relative phase shift need not be 90° . Typically, the loss in a dielectric beam splitter is negligible, assuming that its second surface is antireflection coated. However, the loss in a single-mode fiber coupler may be several dB.

In Appendix A, the following bound is found for a lossy, symmetric, 1:1 output-power-split coupler.

$$\arccos\left(1 - \frac{1}{\text{LOSS}}\right) \leq \phi \leq \arccos\left(\frac{1}{\text{LOSS}} - 1\right) \quad (25)$$

This bound holds for losses less than 3 dB ($0.5 \leq \text{LOSS} \leq 1$). Figure 5 shows this bound on ϕ as a function of coupler loss for a symmetric, 1:1 output-power-split coupler.

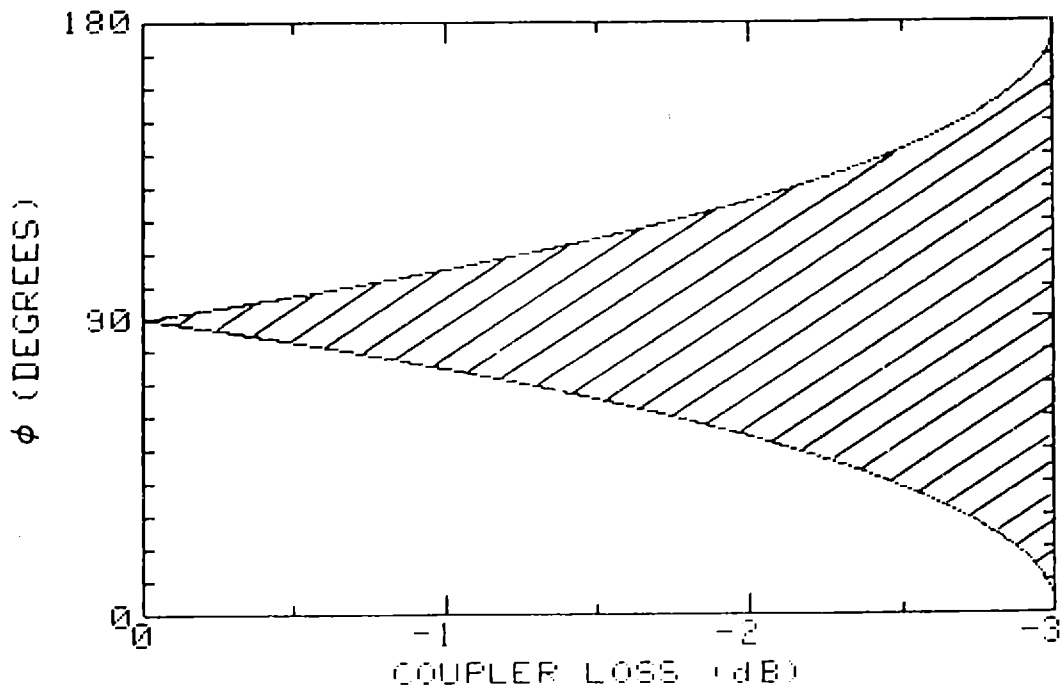


Figure 5: Constraint on a lossy coupler's phase shift.

A value of $\phi \neq 90^\circ$ implies that the I.F. beat signals in the two detectors will not be exactly 180° out of phase. The beat signals are in fact 2ϕ out of phase. Assuming that the I.F. signals in the two detectors are equal in magnitude, figure 6 shows the signal degradation after subtraction as a function of ϕ relative to the case $\phi = 90^\circ$ (0 dB).

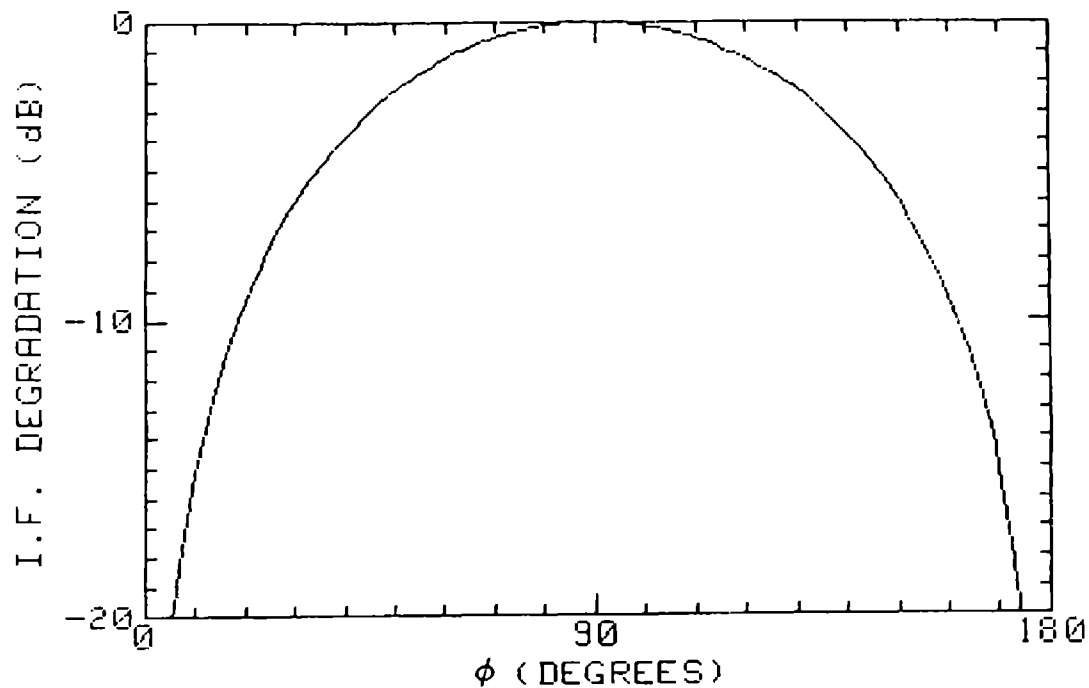


Figure 6: I.F. signal degradation due to $\phi \neq 90^\circ$.

$$\text{I.F. DEGRADATION} = 10 \cdot \log_{10} \left(\frac{1 - \cos(2\phi)}{2} \right) \text{ dB} \quad (26)$$

By combining equations 25 and 26, a bound on signal degradation as a function of coupler loss can be found. For $0.5 \leq \text{LOSS} \leq 1$,

$$\text{I.F. DEGRADATION} \geq 10 \cdot \log_{10} \left(\frac{2 \text{ LOSS} - 1}{\text{LOSS}^2} \right) \text{ dB} \quad (27)$$

Figure 7 shows a plot of this bound as a function of LOSS. A coupler with a loss much greater than 1 dB could potentially give rise to several dB of I.F. signal degradation. This could be a serious problem for single-mode fiber couplers. Any attempt to adjust the phase of one of the I.F. signals will also change the phase of the intensity noise, thereby disrupting the noise cancellation. L.O. noise cancellation is not affected by loss in the coupler, only the I.F. beat signals are.

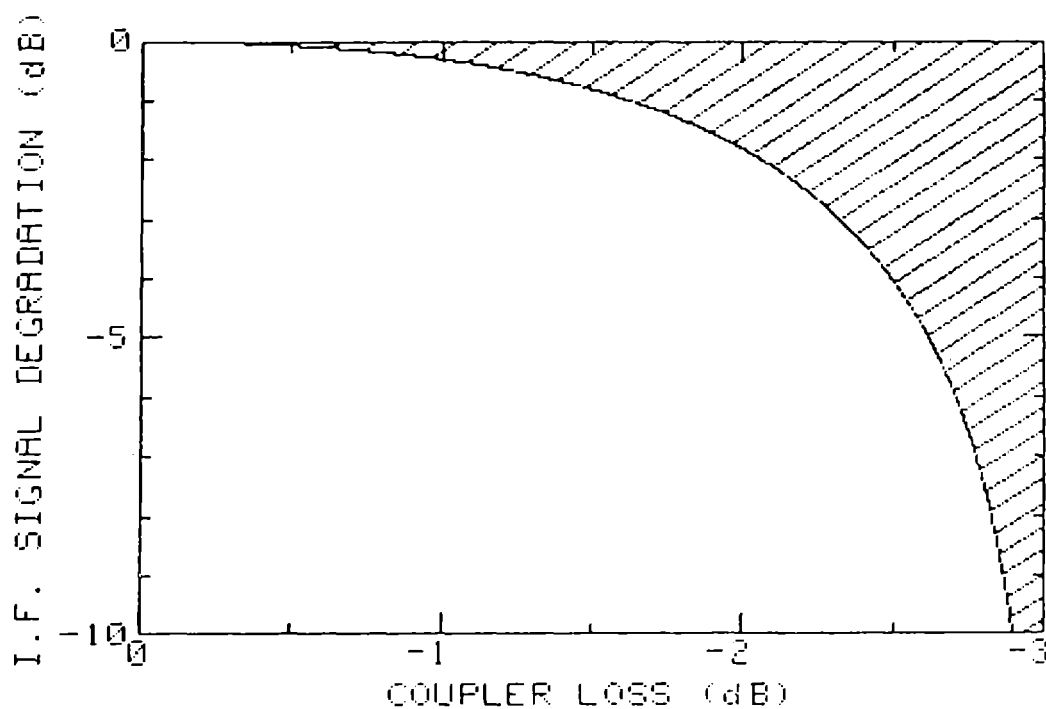


Figure 7: Possible I.F. signal degradation vs. coupler loss.

Chapter III

EXPERIMENTAL RESULTS

In the preceding chapter, the performance of a dual-detector receiver was predicted. In this chapter, that analysis will be verified by experimental results. Several experiments were performed.

The first experiment used a relatively large-area (5.1 mm^2), small-bandwidth (200 MHz) silicon PIN photodetector and unguided laser beams. This experiment demonstrated cancellation of photocurrent noise due to relatively low frequency intensity fluctuations in the L.O. field and verified the enhancement of the I.F. beat signal power as predicted by the analysis [11].

In the second experiment, a delay was added to one branch of the dual-detector receiver. Its effect on L.O. noise cancellation was demonstrated [11].

The third experiment used small-area (0.01 mm^2), large-bandwidth ($>3 \text{ GHz}$) silicon PIN photodetectors to extend the noise cancellation measurements out to 3 GHz. The laser beams were unguided. It was demonstrated that noise at the relaxation resonance frequency of a semiconductor laser ($\sim 1\text{--}10 \text{ GHz}$) could be effectively canceled by the dual-detector receiver [17].

The fourth experiment used single-mode optical fiber to guide the laser beams. A directional fiber coupler was used rather than a beam splitter to combine the received signal and local oscillator beams. The small-bandwidth, large-area photodetectors of the first experiment were used to simplify the noise cancellation measurements. Excess noise cancellation and I.F. beat signal enhancement were demonstrated. Several difficulties were encountered due to non-ideal operation of the fiber coupler.

3.1 UNGUIDED DUAL-DETECTOR RECEIVER

3.1.1 SMALL-BANDWIDTH DETECTORS

3.1.1.1 MATCHED PATH LENGTHS

The apparatus for the unguided dual-detector receiver experiments using small-bandwidth detectors is shown in Fig. 8. The GaAlAs semiconductor laser diode was a Hitachi HLP1400 which lased at approximately 8300 angstroms. The laser bias current of 125 mA was supplied by a battery pack. The laser was enclosed in a thermal housing which stabilized its temperature to $\pm 10^{-3}$ °C. The output beam had an optical power of 13 mW. The laser beam was directed through an acousto-optical modulator to produce a weaker secondary beam whose frequency was offset from the main beam by 80 MHz. The main beam, with frequency at f_0 , was used as the local oscillator. The secondary beam, at $f_0 + 80$ MHz, was used as the received signal beam. The two beams were passed through an optical attenuator. This attenuator provided for variable local oscillator and received signal beam power levels without changing the laser operating point. Changing the attenuation did not significantly change the optical feedback to the laser diode or its excess intensity noise characteristics. The two beams were combined with a 55/45 beam splitter⁹ and mixed in two silicon PIN detectors (5.1 mm², 200 MHz) to obtain the photocurrents I_1 and I_2 . For these experiments, the SNDR optimizing gains, $A_{1,OPT}$ and $A_{2,OPT}$, were not implemented.

The two photocurrents were subtracted with a microwave hybrid junction (Fig. 9). The hybrid junction is a passive four-port device which takes two inputs, I_1 and I_2 , and produces two outputs. Neglecting a small insertion loss, the output from the 0°-0° port is $(I_1 + I_2)/\sqrt{2}$, and the output from the 0°-180° port is $(I_1 - I_2)/\sqrt{2}$. The output from the 0°-180° port of the hybrid junction was then amplified and sent to a spectrum

⁹ The beam splitter was nominally 50/50. Since it was actually measured to be 55/45 ($\epsilon=0.55$), $A_{1,OPT}=(1-\epsilon)/\epsilon=0.82=-1.7$ dB and $A_{2,OPT}=1$ assuming $N_{th}=0$ and matched detectors.

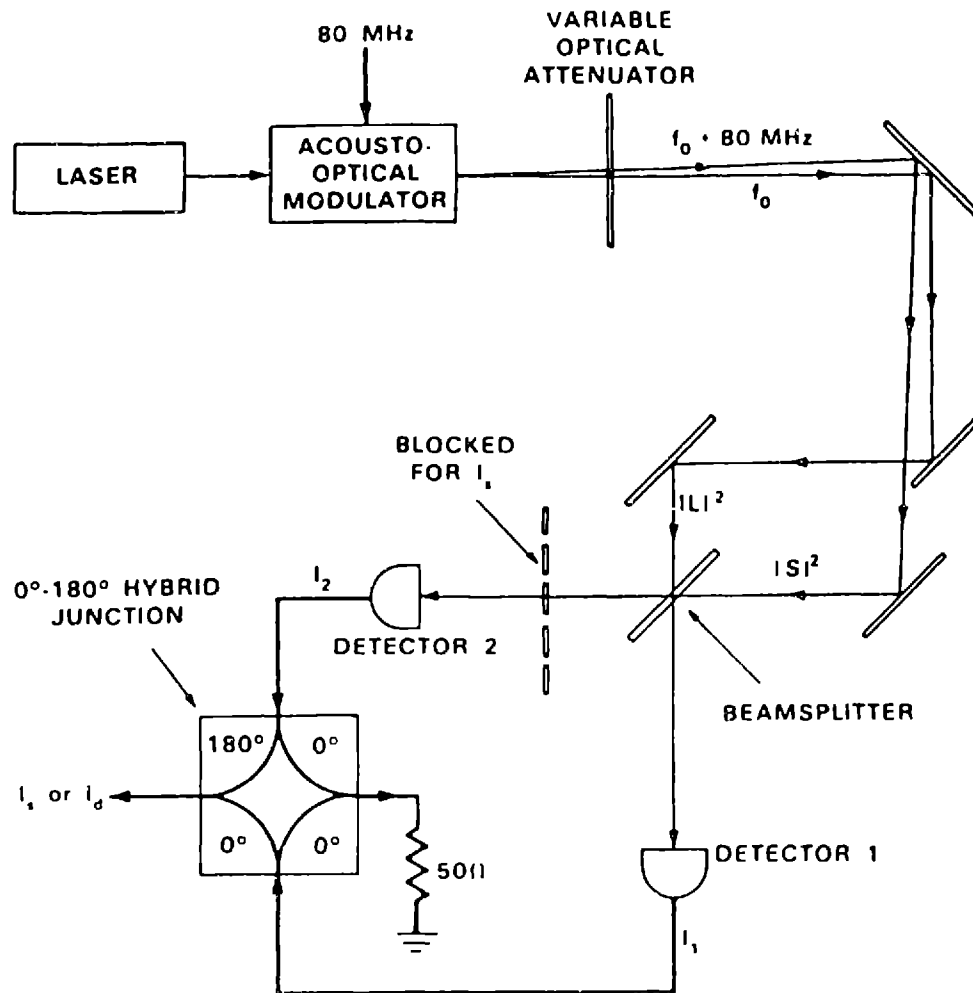


Figure 8: Low-frequency experimental apparatus.

analyzer. Spectra were taken for both the conventional single-detector receiver and the dual-detector receiver.

For the single-detector receiver measurements, the combined fields hitting detector 1 produced I_1 containing a beat signal and noise with a D.C. component of 1.93 mA. The beam normally hitting detector 2 was blocked so that $I_2=0$. I_1 was passed through the hybrid junction to obtain the single-detector receiver output current I_s .

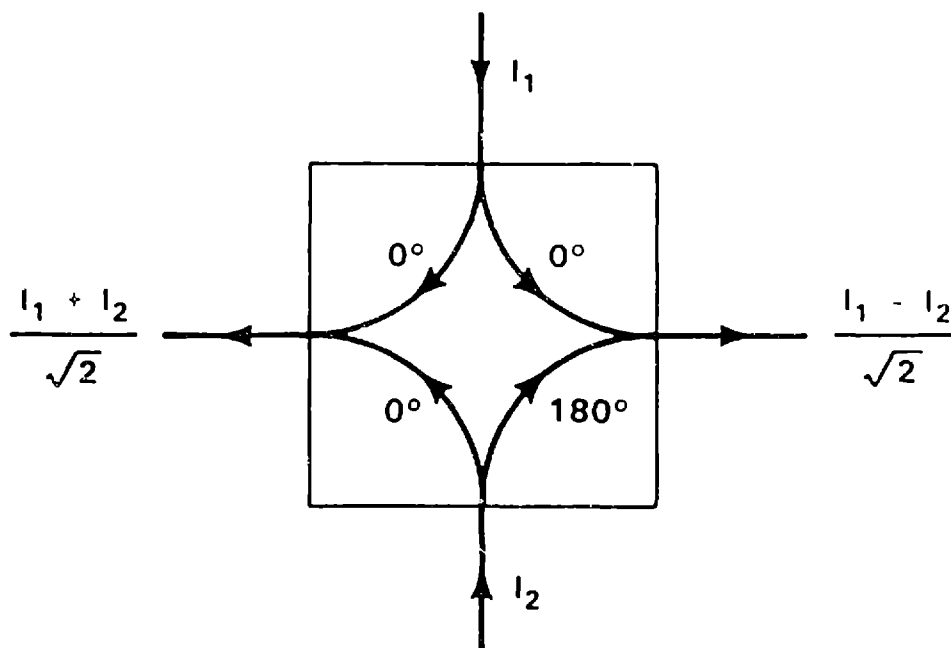


Figure 9: The 0° - 180° microwave hybrid junction.

Due to the hybrid junction, half of the beat signal power and noise power of I_1 are lost. However, this procedure simplifies the comparison between the single- and dual-detector receivers, since it ensures that both have the same insertion losses and detector loads.

For the dual-detector receiver measurements, detector 2 was unblocked. The optical attenuator was adjusted to reduce the laser power so that the sum of the D.C. components of the photocurrents in detectors 1 and 2 (1.10 and 0.83 mA, respectively) equaled the D.C. component of the photocurrent in detector 1 for the single-detector receiver measurements (1.93 mA). The resulting I_1 and I_2 were subtracted with the hybrid junction to obtain the dual-detector receiver output current I_d . Using this procedure, the quantum noise levels for the two receivers are equal if the detector frequency responses are matched.

The ratio of the 80 MHz Beat Signal Powers for the dual- and single-detector receivers (BSP_D and BSP_S , respectively) is:

$$\frac{BSP_D}{BSP_S} = \left[\frac{\epsilon(\eta_1 + \eta_2)}{\epsilon\eta_1 + (1-\epsilon)\eta_2} \right]^2 \quad (28)$$

The ratio of the local oscillator Excess Noise Power Density terms for the two receivers ($ENPD_D$ and $ENPD_S$) is:

$$\frac{ENPD_D}{ENPD_S} = \left[\frac{\eta_1\epsilon - \eta_2(1-\epsilon)}{\eta_1\epsilon + \eta_2(1-\epsilon)} \right]^2 \quad (29)$$

The measured parameters for the experimental setup were $\eta_1=0.84$, $\eta_2=0.83$, and $\epsilon=0.55$. For Hitachi HLP1400 series lasers, typical values for γ at 20 MHz range from 10^2 to 10^3 A⁻¹. For the particular laser and bias currents used in this experiment, $\gamma=10^3$ A⁻¹ at 20 MHz. This value of γ would imply that for a detector with 1 mA of D.C. photocurrent, the excess photocurrent noise power density would be equal to the quantum shot noise power density. Thus, the total noise power density would be 3 dB above the quantum shot noise density.

The quantum shot noise level was found by shining an incoherent white light source on the detectors. The noise produced in the detectors in this manner is quantum limited [19].

The amplifier thermal noise was measured with the light inputs to both detectors blocked. The resulting noise power density was assumed to be independent of all other noise power densities. Therefore, it could be subtracted from the other traces to obtain the noise power densities due to shot noise and local oscillator intensity fluctuations.

Figure 10 shows the experimental noise cancellation data for the above setup with equal optical and electrical path lengths for each receiver branch. The upper trace shows the noise floor for the single-detector receiver. The middle trace shows the noise floor for the dual-detector receiver. The lowest trace shows the quantum noise level for 1.93 mA. All three traces have had the thermal noise of the amplifier removed. For the noise floor measurements, the laser beam was not modulated. The experimental ratios of the 80 MHz beat signals and the 20 MHz noise floors yielded:

$$\frac{BSP_D}{BSP_S} = +0.4 \text{ dB} \quad (30)$$

$$\frac{ENPD_D}{ENPD_S} = -14 \text{ dB} \quad (31)$$

For the measured values of η_1 , η_2 , and ϵ , equations 28 and 29 predict the following theoretical results:

$$\frac{BSP_D}{BSP_S} = +0.8 \text{ dB} \quad (32)$$

$$\frac{ENPD_D}{ENPD_S} = -20 \text{ dB} \quad (33)$$

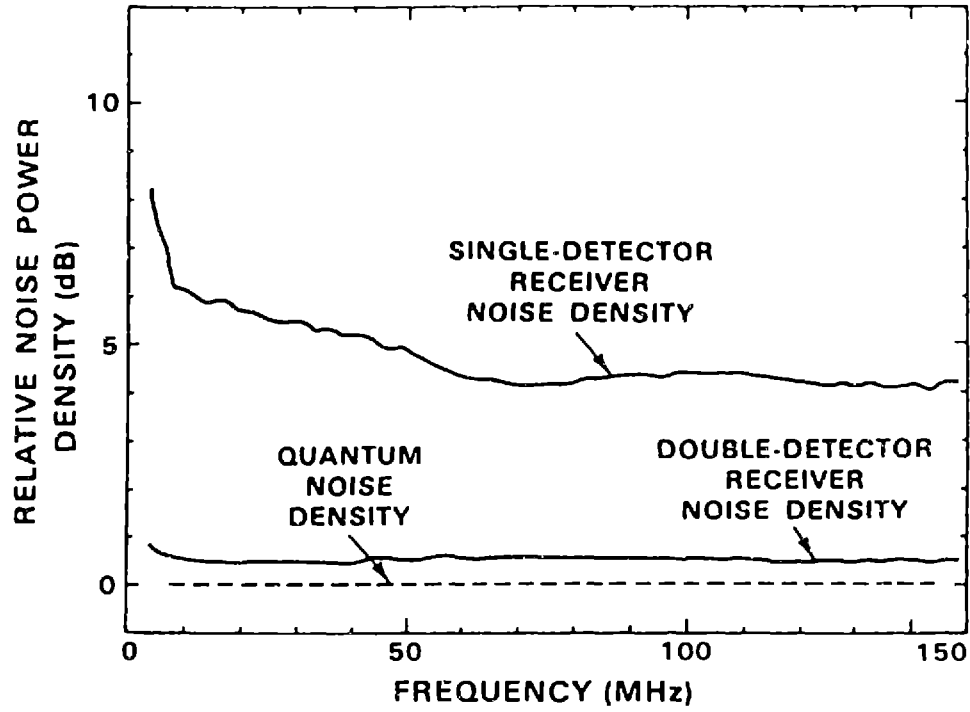


Figure 10: Low-frequency intensity noise cancellation data (no delay).

As predicted, the two beat signals did add constructively, whereas the local oscillator excess intensity noise was substantially suppressed. There is a discrepancy between the amounts of cancellation observed and predicted. This discrepancy could be due to errors in measuring the beam splitter transmission and the detector quantum efficiencies. Clearly, since the D.C. photocurrents are given by the expressions

$$I_1 = \frac{\epsilon \eta_1}{\hbar \omega} |L|^2 \text{ and } I_2 = \frac{\epsilon \eta_2}{\hbar \omega} |L|^2,$$

$$\frac{\epsilon \eta_1}{(1-\epsilon) \eta_2} = \frac{(0.55)(0.84)}{(0.45)(0.83)} = 1.24 \quad (34)$$

should equal

$$\frac{I_1}{I_2} = \frac{1.10}{0.83} = 1.33 \quad (35)$$

so there was indeed a measurement error somewhere. Rewriting Eq. 29 in terms of the D.C. photocurrents:

$$\frac{\text{ENPD}_D}{\text{ENPD}_S} = \left[\frac{I_1 - I_2}{I_1 + I_2} \right]^2 = -17 \text{ dB} \quad (36)$$

17 dB of cancellation was in fact observed for several runs of the experiment. It was also later discovered that the local oscillator's excess noise floor was slowly varying with time. This variation was several dB in magnitude with a period on the order of a few minutes. Such a variation could account for the range of 14 to 17 dB of cancellation observed.

The discrepancy between the actual and predicted levels of cancellation could also be due to errors in the measurement of the detector quantum efficiencies. It is very difficult to accurately measure a detector's quantum efficiency, which can be strongly affected by alignment, tilt, multiple reflections, etc.

3.1.1.2 UNMATCHED PATH LENGTHS

The effect of unmatched signal path lengths in the two branches of the dual-detector receiver was measured by inserting a long coaxial cable between detector 1 and the hybrid junction.¹⁰ The delay of the cable was found by taking one half of the

¹⁰ The effect of a differential electrical delay is identical to the effect of an equal differential optical delay.

round trip time of a pulse injected in one end of the cable with the opposite end shorted. The one-way delay was measured to be $T=15.4$ ns ($1/T=65$ MHz). The noise cancellation data for the dual-detector receiver with unmatched path lengths is shown in figure 11. The data displays the $1-\cos(2\pi fT)$ dependence of the excess noise cancellation.

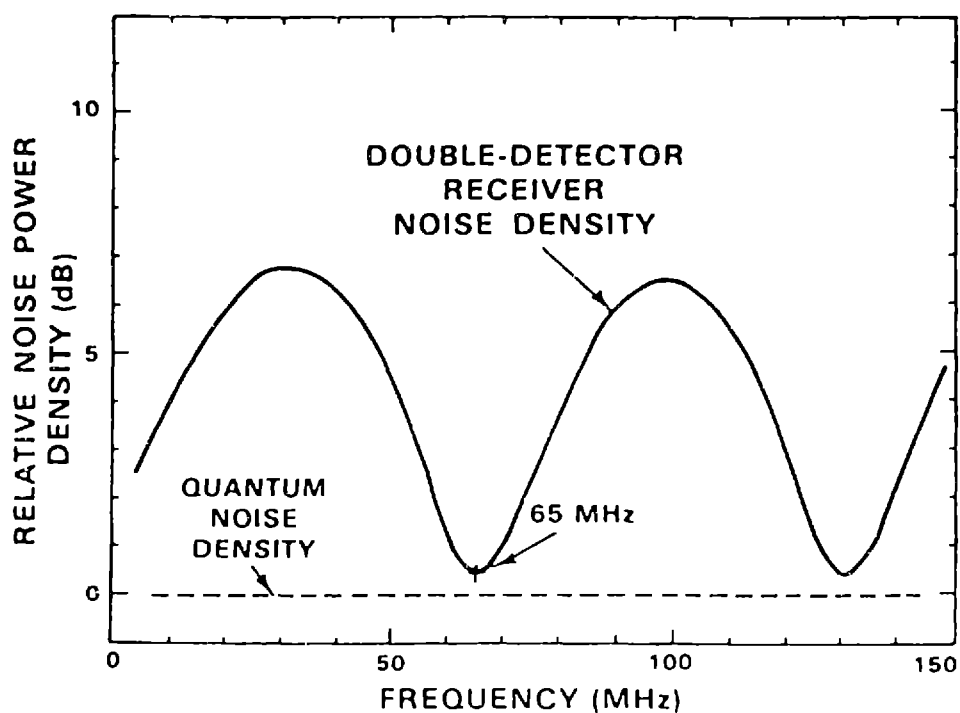


Figure 11: Noise cancellation data with delay.

Although this data corresponds to an extreme difference in length between the two signal paths, it demonstrates the requirement of near equal path lengths (<1 cm difference) if 20 dB of L.O. intensity noise cancellation is desired for frequencies up to 1 GHz.

3.1.2 LARGE-BANDWIDTH DETECTORS

The intensity noise of semiconductor lasers is not flat beyond 150 MHz as figure 10 might suggest. There is a strong broad-band resonance (typically 10's of dB above the 10–100 MHz noise floor) in the intensity noise spectrum which peaks at a frequency on the order of 1 to 10 GHz [13]. The low-frequency tail of the resonance can severely degrade a conventional wide-band single-detector heterodyne receiver's performance. However, the dual-detector receiver can cancel this resonance.

The apparatus used for the experiment to demonstrate high-frequency L.O. noise cancellation is shown in figure 12. It was similar to the low-frequency apparatus, except that the detectors were replaced with smaller-area (0.01 mm²), larger-bandwidth (>3 GHz) PIN silicon detectors.

The measurements were taken as follows. A Hitachi HLP1400 was biased at 64.5 mA ($I/I_{th}-1=0.071$). The relaxation resonance frequency, f_r , for this diode was given by the relationship $f_r=6.01(I/I_{th}-1)^{1/2}$ GHz. Thus, the peak of the relaxation resonance was at 1.5 GHz. The laser (L.O.) beam was blocked periodically by a chopper which also provided a frequency and phase reference to a lock-in amplifier. The L.O. beam was split with a 55/45 beam splitter. The acousto-optical modulator was not used, and no attempt was made to demonstrate I.F. signal enhancement. The D.C. photocurrents in detectors 1 and 2 after chopping were 9.9 and 9.3 microamps, respectively. The photocurrents produced in the two detectors were subtracted, amplified, and sent to the spectrum analyzer. The spectrum analyzer was set to linear mode and its video output (proportional to amps/Hz^{1/2}) was sent to a D.C. coupled squaring amplifier. The output from the squarer (proportional to amps²/Hz) was sent to the lock-in amplifier. The function of the lock-in amplifier was to produce an output proportional to the part of its input which was at the chop frequency and phase. The lock-in output was proportional to the difference in photocurrent noise power density

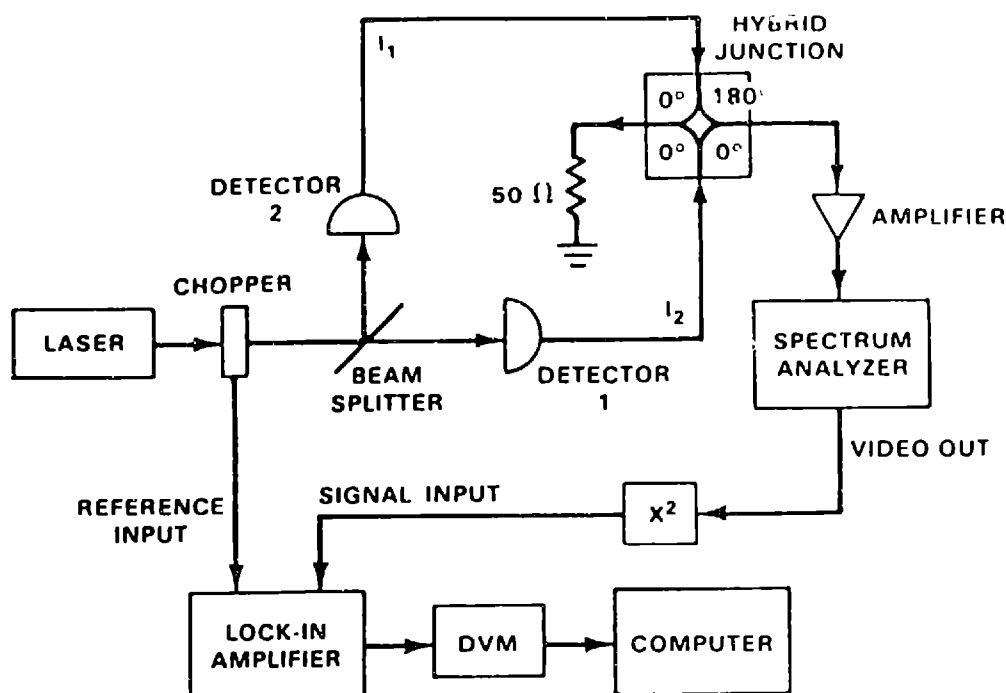


Figure 12: High-frequency experimental apparatus.

produced while the laser beam was blocked and unblocked. This was the desired information, with the additional benefit that the amplifier thermal noise was automatically removed from the data. The measurement sensitivity was increased enough that the shot noise of a few microamps could be accurately measured. Without the lock-in, a few hundred microamps of D.C. photocurrent was needed to make the shot noise visible over the thermal noise.

L.O. intensity noise spectra were taken for both a single-detector receiver (detector 1) and the dual-detector receiver with subtraction. Calibration of the apparatus was obtained by illuminating each detector with an incoherent white light source. The in-

tensity of the white light source was adjusted to produce the same D.C. photocurrents in the two detectors as the laser had. The photocurrent noise produced in this manner was quantum-limited. The laser intensity noise spectra were normalized by the quantum shot noise spectra. The spectra for the single-detector receiver (at $9.9 \mu\text{A}$) was scaled to correspond to the noise power density that would have been observed if the D.C. photocurrent was equal to that of the dual-detector receiver (at $19.2 \mu\text{A}$).¹¹ The results are shown in figure 13. The upper trace is the photocurrent noise power density of the scaled single-detector receiver. The lower trace (labeled "DUAL-DETECTOR RECEIVER") is the noise power density after cancellation. 0 dB on the plot is the quantum noise power density. The excess noise power density has been reduced by >20 dB over most of the frequency range. The total noise power density is <3 dB above the quantum limit at the relaxation resonance peak. The increase in the noise floor at 1.5 GHz is due to mismatch of the two detectors' frequency responses. The third trace (labeled "PREDICTED CANCELLATION") shows the predicted noise floor of the dual-detector receiver based on the noise floor of the single-detector receiver, the detector photocurrents, and the measured detector frequency responses (see figure 14).

Figure 14 was obtained from the quantum shot noise measurements for each detector. The two detectors' responses are matched within 1 dB until about 1.5 GHz. At that frequency and beyond, the mismatched is often greater than 2 dB and poor cancellation is expected (see Section 2.6).

¹¹ The scaling was done as follows: Subtract 1 from the ratio of laser intensity noise density to shot noise density. Multiply this quantity by $(19.2 \text{ mA}/9.9 \text{ mA})^2$ and add 1.

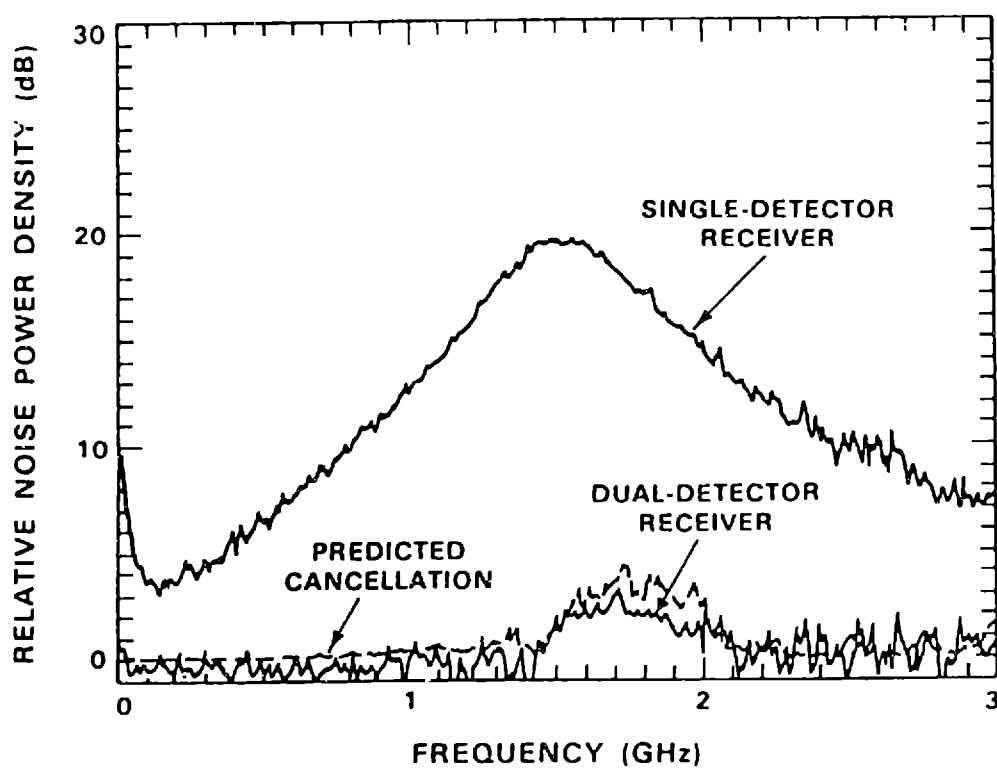


Figure 13: High-frequency noise cancellation data.

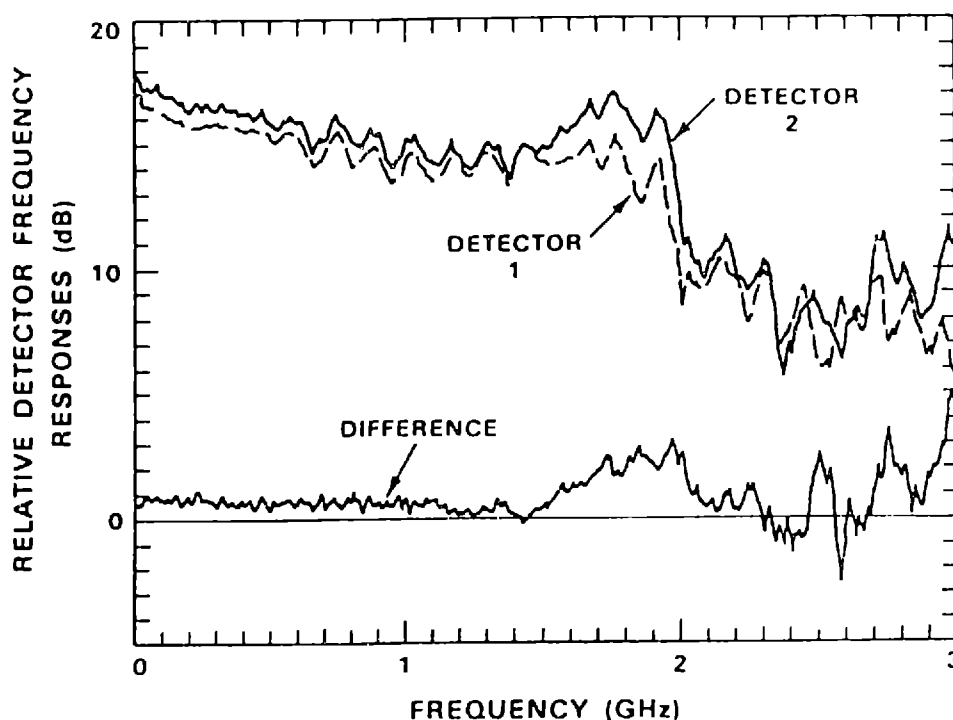


Figure 14: The measured detector frequency responses.

3.2 GUIDED DUAL-DETECTOR RECEIVER

In this section, the results of an attempt to demonstrate local oscillator intensity noise suppression in single-mode fiber are presented. The experimental apparatus was identical to that of the unguided, low-frequency measurements (Section 3.1.1), except that the beam splitter was replaced by a directional fiber coupler (Figure 15) [14,15].

The function of the fiber coupler is similar to that of a beam splitter. Light from the local oscillator beam (L) and from the received signal beam (S) are focused into the coupler's inputs, 1 and 2.¹² The coupler takes the energy in each input and splits

¹² In a real system, the signal beam would have been focused into the fiber at the transmitter end of the link.

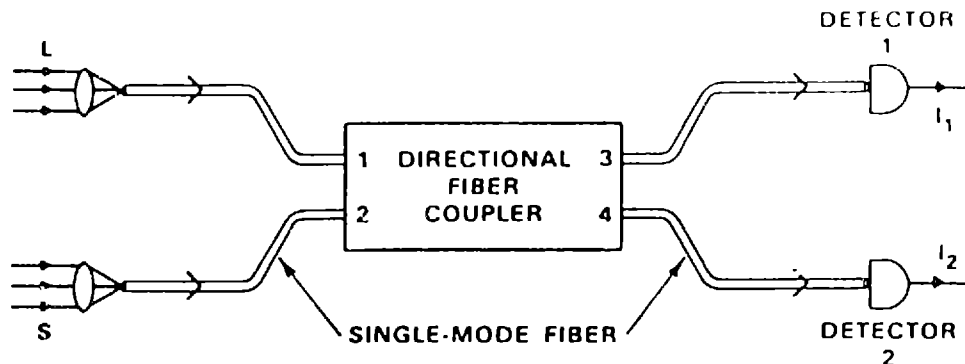


Figure 15: The single-mode fiber directional coupler.

is according to some ratio which depends on the coupler's construction, the input polarization, and the input wavelength. The outputs, 3 and 4, which contain some fraction of each input, are mixed in the detectors to produce the heterodyne beat signals.

If the coupler is lossless and symmetric, it will perform the same function as a beam splitter. Unfortunately, practical couplers typically have a few dB of insertion loss. Since the coupler is lossy, the two heterodyne beat signals need not be 180° out of phase (see Appendix A).

The insertion loss of the coupler used in the experiment was estimated to be -8 dB. This value was obtained by comparing the power that could be coupled into a short length of the single-mode fiber with the sum of the powers that could be coupled into port 1 and output from ports 3 and 4. The maximum coupling efficiency observed through a normal piece of fiber was 0.30. The maximum efficiency observed through the fiber coupler was 0.044. Thus, the insertion loss is given by $10 \log_{10}(0.044/0.30) = -8$ dB.

With this large value of insertion loss, the bound on the relative phase shift between the two output ports is useless. The actual phase shift was measured by using the following technique (see figure 16). The laser beam was sent through the acousto-optical modulator to produce a secondary beam offset in frequency by 80 MHz from the main beam. The main beam was focused into input port 1 of the coupler. The secondary beam was focused into input port 2. The fiber end faces had been cleaved by a method similar to that described in [16]. The coupler outputs 3 and 4, when placed on detectors 1 and 2, produced 80 MHz I.F. signals with phases ϕ_3 and ϕ_4 , respectively. The two signals were individually amplified and sent to a dual-trace oscilloscope where the difference in phase between the two signals could be measured. Assuming that the amplifiers and cables give phase shifts to the signals as shown in the illustration, the measured phase difference ϕ' equals:

$$\phi' = \phi_3 + \phi_A + \phi_C - \phi_4 - \phi_B - \phi_D \quad (37)$$

Next, fibers 3 and 4 were interchanged and the phase difference ϕ'' was measured with the scope. The detectors and other electronics were not changed. Thus:

$$\phi'' = \phi_4 + \phi_A + \phi_C - \phi_3 - \phi_B - \phi_D \quad (38)$$

The phase difference between the I.F. signals at the detectors is then:

$$\phi_3 - \phi_4 = \frac{\phi' - \phi''}{2} \quad (39)$$

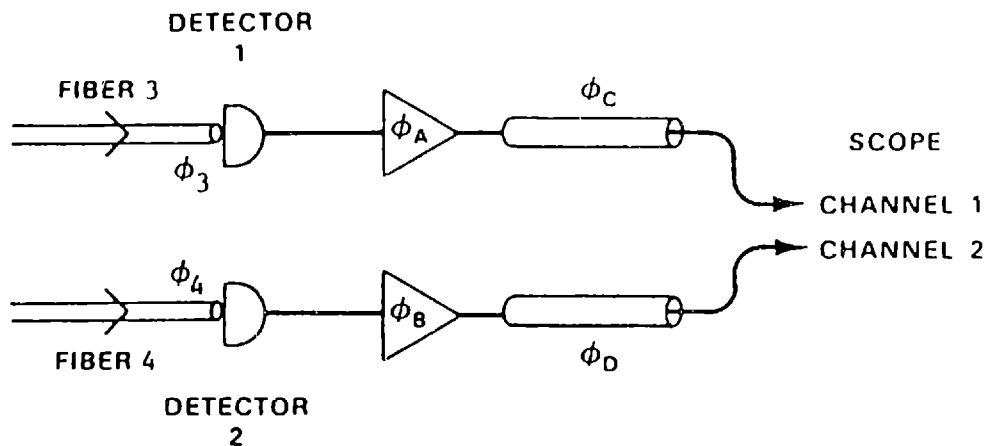


Figure 16: Measurement of I.F. signal phase difference.

The measured values were $\phi' = 243^\circ$ and $\phi'' = 139^\circ$. This yields a value of $\phi_3 - \phi_4 = 52^\circ$. The value of $\phi_3 - \phi_4$ is arbitrary to a multiple of 180° . As shall be shown later in this section, the I.F. signals were found to add constructively, which would imply that $\phi_3 - \phi_4 = -128^\circ$.

The apparatus was modified to include the hybrid junction for subtraction of the two photocurrents. The results of measuring the amplitudes of the individual beat signals in detectors 1 and 2 (a and b, respectively) and their difference (c) are shown in figure 17. These measurements give another estimate of the I.F. phase difference, since by the law of cosines:

$$c^2 = a^2 + b^2 - 2ab \cdot \cos(\phi_3 - \phi_4) \quad (40)$$

$$\phi_3 - \phi_4 = \arccos \left(\frac{a^2 + b^2 - c^2}{2ab} \right) \quad (41)$$

$a=2.43$ mV, $b=1.74$ mV, and $c=3.92$ mV gives:

$$\begin{aligned} \phi_3 - \phi_4 &= \arccos(-0.76) \\ &= \pm 140^\circ \end{aligned} \quad (42)$$

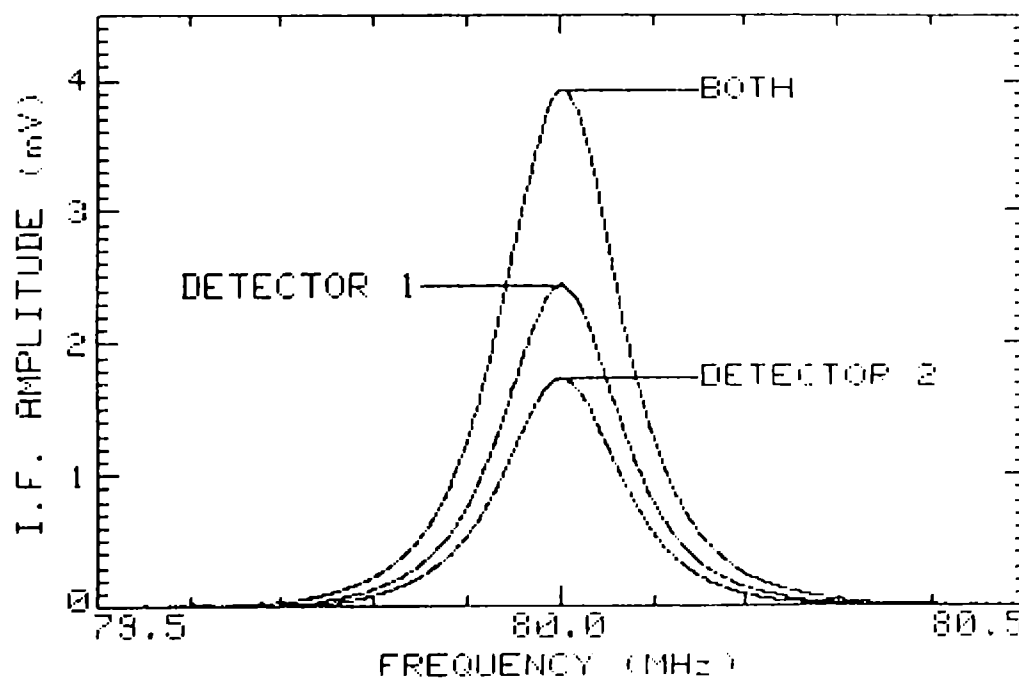


Figure 17: 80 MHz I.F. signal enhancement data.

This value agrees fairly well with the previous estimate of -128° .

The individual signal levels of the two detectors were not equal. This implies that the fiber coupler was not a symmetric device, since the detectors were well-matched.

Let the scattering matrix of the coupler be given by T so that:

$$\begin{bmatrix} E_3 \\ E_4 \end{bmatrix} = \underbrace{\begin{bmatrix} T_{31} & T_{32} \\ T_{41} & T_{42} \end{bmatrix}}_T \begin{bmatrix} E_1 \\ E_2 \end{bmatrix} \quad (43)$$

The measured magnitudes of the scattering matrix coefficients were:

$$\begin{aligned} |T_{31}|^2 &= 5.0 \times 10^{-3} & |T_{32}|^2 &= 8.5 \times 10^{-3} \\ |T_{41}|^2 &= 42.6 \times 10^{-3} & |T_{42}|^2 &= 6.1 \times 10^{-3} \end{aligned} \quad (44)$$

$$\begin{aligned} \text{OUTPUT POWER SPLIT FOR INPUT PORT 1} &\rightarrow 8.5:1 \\ \text{OUTPUT POWER SPLIT FOR INPUT PORT 2} &\rightarrow 1.4:1 \end{aligned} \quad (45)$$

The output power splits were found to be extremely sensitive to the input polarization. The optical fiber used in the coupler was not polarization preserving fiber. Bending the fiber or moving the coupler could drastically change the output power splits. The inputs to the fiber were identical in polarization. However, after traveling through the ~ 40 cm fiber pigtails to the coupler, the two input polarizations may have been changed significantly. This could result in the asymmetric power split observed.

The output from port 2 with input to port 1 was measured for the fiber coupler. 7.4×10^{-3} of the power input to port 1 was found to leak out port 2. This level of iso-

lation could possibly cause the local oscillator to beat with itself due to multiple reflections in the coupler. The local oscillator noise produced in the two detectors in this manner would be 180° out of phase and thus increase when subtracted rather than cancel.

Though the beat signal enhancement does depend on loss in the coupler, the L.O. noise cancellation property of the dual-detector receiver does not. For the noise floor measurements, the acousto-optical modulator was turned off. The D.C. photocurrents in detectors 1 and 2 were 50 and 8 microamps, respectively, implying a 6:1 output-power-split ratio for the local oscillator input. With this split and no scaling gains or attenuators, the expected L.O. noise cancellation is (from Eq. 36):

$$10 \log_{10} \left(\frac{6 - 1}{6 + 1} \right)^2 = -3 \text{ dB} \quad (46)$$

Figure 18 shows the L.O. intensity noise cancellation data for the fiber coupler dual-detector heterodyne receiver. The upper trace is the data for detector 1 (at 50 μA) scaled to correspond to the noise in a single-detector receiver with a photocurrent of 58 μamps (see Section 3.1.2). The lower trace is the dual-detector receiver noise floor at 58 μamps . 0 dB is the quantum noise level. The rise in intensity noise at 160 MHz is due to feedback into the laser cavity from the measurement apparatus. The data does show a 3 dB decrease in the noise floor as predicted.

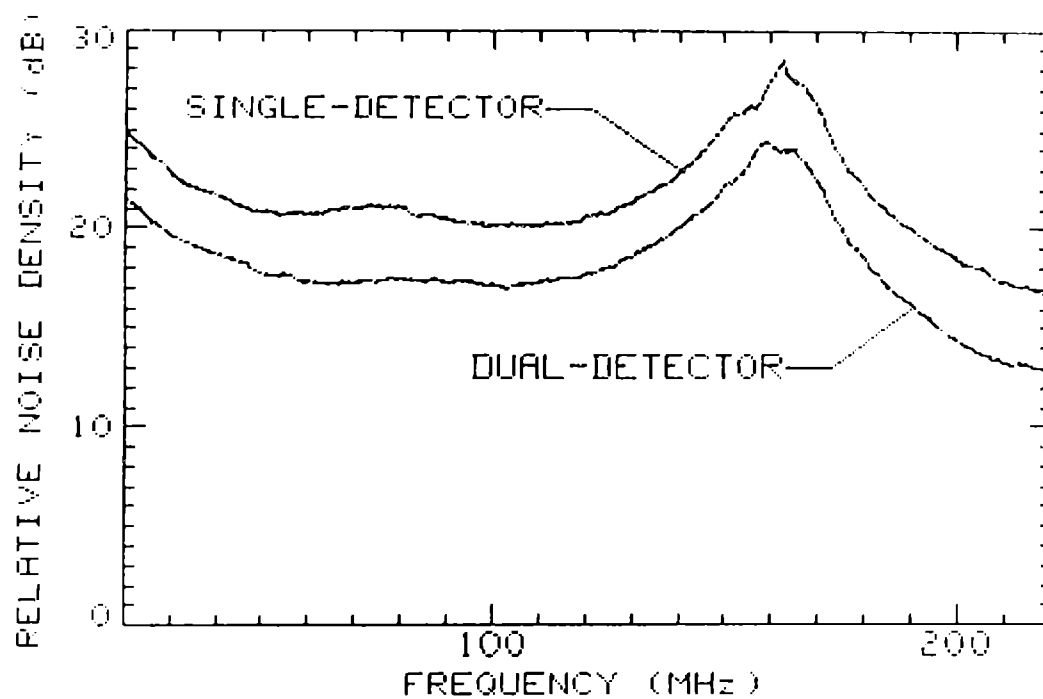


Figure 18: Noise cancellation data in optical fiber.

Chapter IV

CONCLUSIONS

The dual-detector optical heterodyne receiver possesses two main advantages over the conventional single-detector heterodyne receiver — increased performance and reduced local oscillator power requirements.

First, the dual-detector heterodyne receiver can provide near-quantum-limited performance in the presence of severe intensity fluctuations that might substantially degrade a single-detector receiver's performance. This is due to the L.O. intensity noise cancelling nature of the balanced receiver. Not only does this property increase performance, it also increases the receiver's robustness. The receiver's performance is insensitive to changes in the local oscillator's noise characteristics, which may result, for example, due to aging.

Second, the dual-detector heterodyne receiver is able to achieve this improved performance and robustness with much less local oscillator power. Since both beam splitter outputs are collected, no L.O. power is wasted, as opposed to a single-detector receiver where typically more than 90% of the local oscillator power is discarded. This property is very important if the receiver's local oscillator is power-limited.

The increase in complexity of the dual-detector receiver over the single-detector receiver required to achieve these advantages is minimal. The phase fronts of the two fields in ^{the} second beam splitter output are already aligned. All that is required is to find a well-matched second detector to collect it. The subtraction of the two photocurrents is not difficult. No scaling attenuators are necessary if the beam splitter is 50/50 and the detectors are matched.

For optimum performance and 20 dB of local oscillator noise cancellation, the dual-detector receiver should use a 50/50 beam splitter (or coupler) with less than 1 dB power loss. The beam splitter should be kept as close to 50/50 as possible (better than 45/55) to prevent the need of scaling attenuators. Signal path lengths must be matched (to within a few millimeters for a 1 GHz receiver). And finally, it is necessary to have two detectors matched to within 1 dB — both in quantum efficiency and frequency response.

If a communication system is to make use of optical heterodyne technology and use a local oscillator which is noisy or power-limited, the dual-detector receiver is far preferable to the conventional single-detector receiver.

Appendix A

COUPLER PHASE SHIFTS

Figure 19 shows a four-port device with two inputs and two outputs. If the device is linear and symmetric, each input is coupled to both outputs with a resulting magnitude change and phase shift. The coupling coefficients can be represented by two unknown complex constants, A and B, such that for two arbitrary complex inputs S and L, the resulting outputs are $AS+BL$ and $BS+AL$.

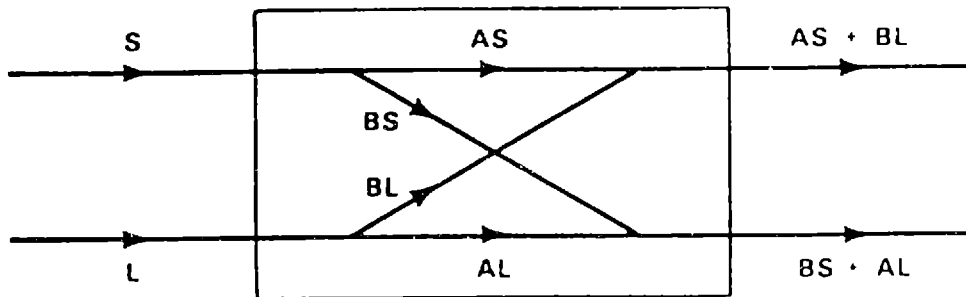


Figure 19: Symmetric, linear, four-port coupler.

The transformation of the coupler is given by:

$$\begin{bmatrix} \text{OUT}_1 \\ \text{OUT}_2 \end{bmatrix} = \underbrace{\begin{bmatrix} A & B \\ B & A \end{bmatrix}}_T \begin{bmatrix} S \\ L \end{bmatrix} \quad (47)$$

Let $A = ae^{j\phi_r}$ and $B = be^{j\phi_t}$. Then

$$T = \begin{bmatrix} ae^{j\phi_r} & be^{j\phi_t} \\ be^{j\phi_t} & ae^{j\phi_r} \end{bmatrix} \quad (48)$$

$$= \begin{bmatrix} a & be^{j\phi} \\ be^{j\phi} & a \end{bmatrix} e^{j\phi_r} \quad (49)$$

where $\phi = \phi_t - \phi_r$.

$$T^+ T = \begin{bmatrix} a^2 + b^2 & 2ab \cdot \cos \phi \\ 2ab \cdot \cos \phi & a^2 + b^2 \end{bmatrix} \quad (50)$$

If the coupler is lossless, $T^+ T = I$ for power conservation.¹³ Thus, $\phi = \pm 90^\circ$ and $a^2 + b^2 = 1$.

Whether or not the coupler is lossless, the matrix $I - T^+ T$ must be positive semi-definite. This is equivalent to the statement that there is no power gain due to the transformation. With this constraint, it can be shown that the magnitudes of the eigenvalues of T are both ≤ 1 (the eigenvalues of the identity matrix).

Let v_1 and v_2 be normalized eigenvectors of T such that:

$$\begin{aligned} T v_1 &= \lambda_1 v_1 & T v_2 &= \lambda_2 v_2 \\ v_1^+ v_1 &= 1 & v_2^+ v_2 &= 1 \end{aligned} \quad (51)$$

¹³ T^+ represents the transpose conjugate of T .

Since $I - T^*T$ is positive semi-definite, $v_1^*(I - T^*T)v_1 \geq 0$. But:

$$v_1^* I v_1 - v_1^* T^* T v_1 = 1 - |\lambda_1|^2 \quad (52)$$

Thus, $|\lambda_1| \leq 1$. Similarly, $|\lambda_2| \leq 1$.

The magnitudes of the eigenvalues of T are:

$$|\lambda| = \frac{2ab \cdot \cos \phi}{a^2 + b^2} \quad (53)$$

Thus, for $|\lambda| \leq 1$:

$$\frac{a^2 + b^2 - 1}{2ab} \leq \cos \phi \leq \frac{1 - a^2 - b^2}{2ab} \quad (54)$$

If $(1 - a^2 - b^2)/(2ab) \leq 1$:

$$\arccos\left(\frac{a^2 + b^2 - 1}{2ab}\right) \leq \phi \leq \arccos\left(\frac{1 - a^2 - b^2}{2ab}\right) \quad (55)$$

Otherwise, ϕ is unbounded.

If $a=b$ (i.e. the output power split of the coupler is 1:1), the above expression simplifies to:

$$\arccos\left(1 - \frac{1}{2a^2}\right) \leq \phi \leq \arccos\left(\frac{1}{2a^2} - 1\right) \quad (56)$$

And since $a^2 + b^2 = 2a^2 = \text{LOSS}$:

$$\arccos\left(1 - \frac{1}{\text{LOSS}}\right) \leq \phi \leq \arccos\left(\frac{1}{\text{LOSS}} - 1\right) \quad (57)$$

for $0.5 \leq \text{LOSS} \leq 1$. ϕ is unbounded for $0 \leq \text{LOSS} \leq 0.5$.

Appendix B

SNDR BOUNDS

In this appendix, the bounds on the dual-detector receiver signal-to-noise-density ratio stated in Section 2.2, Eq. 14, are proven.

THEOREM: For all η_1, η_2, ϵ , and β such that $0 < \eta_1 \leq 1$, $0 < \eta_2 \leq 1$, $0 \leq \epsilon \leq 1$, and $0 \leq \beta$:

$$\frac{S^2}{N\omega} \min(\eta_1, \eta_2) \leq \frac{S^2}{N\omega} \text{SNDR}' \leq \frac{S^2}{N\omega} \max(\eta_1, \eta_2) \quad (58)$$

$$\text{where } \text{SNDR}' = \frac{[(1+\eta_2\beta)(1-\epsilon)\eta_1 + (1+\eta_1\beta)\epsilon\eta_2]^2}{(1+\eta_2\beta)^2(1-\epsilon)\eta_1 + (1+\eta_1\beta)^2\epsilon\eta_2 + \beta(\eta_1-\eta_2)^2\epsilon(1-\epsilon)}$$

PROOF: There are three possible cases which must be proven.

- I. $\eta_1 = \eta_2 = \eta$: Show that $\text{SNDR}' = \eta$,
or equivalently that $\text{SNDR}' - \eta = 0$.
- II. $\eta_1 > \eta_2$: Show that $\eta_2 \leq \text{SNDR}' \leq \eta_1$,
or equivalently that $\text{SNDR}' - \eta_2 \geq 0$ and $\text{SNDR}' - \eta_1 \leq 0$.
- III. $\eta_1 < \eta_2$: Show that $\eta_1 \leq \text{SNDR}' \leq \eta_2$,
or equivalently that $\text{SNDR}' - \eta_1 \geq 0$ and $\text{SNDR}' - \eta_2 \leq 0$.

First, find the sign of $\text{SNDR}' - \eta_1$. Since the denominator of SNDR' is always non-negative, the problem reduces to finding the sign of:

$$\text{NUM}(\text{SNDR}') - \eta_1 \cdot \text{DENOM}(\text{SNDR}') \quad (59)$$

Thus, by substituting the expression for SNDR' and regrouping terms according to their order in β , we proceed as follows:

$$\begin{aligned} & [(1-\epsilon)\eta_1 + (1-\epsilon)\eta_1\eta_2\beta + \epsilon\eta_2 + \epsilon\eta_1\eta_2\beta]^2 \\ & - \eta_1 \cdot [(1-\epsilon)\eta_1 + 2(1-\epsilon)\eta_1\eta_2\beta + (1-\epsilon)\eta_1^2\beta^2 + \epsilon\eta_2 + 2\epsilon\eta_1\eta_2\beta \\ & + \epsilon\eta_1^2\beta^2 + \epsilon(1-\epsilon)(\eta_1 - \eta_2)^2\beta] \end{aligned} \quad (60)$$

$$\begin{aligned} & = [(1-\epsilon)\eta_1 + \epsilon\eta_2 + \eta_1\eta_2\beta]^2 \\ & - \eta_1 \cdot [(1-\epsilon)\eta_1 + \epsilon\eta_2 + 2\eta_1\eta_2\beta + \epsilon(1-\epsilon)(\eta_1 - \eta_2)^2\beta \\ & + (1-\epsilon)\eta_1^2\beta^2 + \epsilon\eta_1^2\beta^2] \end{aligned} \quad (61)$$

$$\begin{aligned} & = [(1-\epsilon)\eta_1 + \epsilon\eta_2]^2 + 2[(1-\epsilon)\eta_1 + \epsilon\eta_2]\eta_1\eta_2\beta \\ & + \eta_1^2\eta_2^2\beta^2 - \eta_1 \cdot [\quad " \quad] \end{aligned} \quad (62)$$

$$\begin{aligned} & = \epsilon(\eta_2 - \eta_1)[(1-\epsilon)\eta_1 + \epsilon\eta_2] + \epsilon(\eta_2 - \eta_1)2\eta_1\eta_2\beta - \epsilon(1-\epsilon)\eta_1(\eta_2 - \eta_1)^2\beta \\ & + \epsilon\eta_1^2\eta_2^2\beta^2 - \epsilon\eta_1^3\eta_2\beta^2 \end{aligned} \quad (63)$$

$$= \quad " \quad + \epsilon(\eta_2 - \eta_1)\eta_1\beta[2\eta_2 - (1-\epsilon)(\eta_2 - \eta_1)] + \epsilon\eta_1^2\eta_2\beta^2(\eta_2 - \eta_1) \quad (64)$$

$$= \quad " \quad + \epsilon(\eta_2 - \eta_1)\eta_1\beta[(1+\epsilon)\eta_2 + (1-\epsilon)\eta_1] + \quad " \quad (65)$$

$$= \epsilon(\eta_2 - \eta_1)\{[(1-\epsilon)\eta_1 + \epsilon\eta_2] + \eta_1\beta[(1+\epsilon)\eta_2 + (1-\epsilon)\eta_1] + \eta_1^2\eta_2\beta^2\} \quad (66)$$

Similarly, the sign of $\text{SNDR}' - \eta_2$ is found. Substituting η_2 for η_1 in Eq. 59 and picking up the previous derivation at Eq. 62 yields:

$$[(1-\epsilon)\eta_1 + \epsilon\eta_2]^2 + 2[(1-\epsilon)\eta_1 + \epsilon\eta_2]\eta_1\eta_2\beta + \eta_1^2\eta_2^2\beta^2 - \eta_2 \cdot \uparrow \quad (67)$$

$$= (1-\epsilon)(\eta_1 - \eta_2)[(1-\epsilon)\eta_1 + \epsilon\eta_2] + (1-\epsilon)(\eta_1 - \eta_2)2\eta_1\eta_2\beta - \eta_2\epsilon(1-\epsilon)(\eta_1 - \eta_2)^2\beta + (1-\epsilon)\eta_1^2\eta_2^2\beta^2 - (1-\epsilon)\eta_1\eta_2^3\beta^2 \quad (68)$$

$$= \quad " \quad + (1-\epsilon)(\eta_1 - \eta_2)\eta_2\beta[2\eta_1 - \epsilon(\eta_1 - \eta_2)] + (1-\epsilon)\eta_1\eta_2^2\beta^2(\eta_1 - \eta_2) \quad (69)$$

$$= \quad " \quad + (1-\epsilon)(\eta_1 - \eta_2)\eta_2\beta[(2-\epsilon)\eta_1 + \epsilon\eta_2] \quad + \quad " \quad (70)$$

$$= (\eta_1 - \eta_2)(1-\epsilon)\{[(1-\epsilon)\eta_1 + \epsilon\eta_2] + \eta_2\beta[(2-\epsilon)\eta_1 + \epsilon\eta_2] + \eta_1\eta_2^2\beta^2\} \quad (71)$$

The terms in braces in Eqs. 66 and 70 are non-negative by the assumed constraints on η_1 , η_2 , ϵ , and β . All three cases — I, II, and III — are easily seen to be true, and the theorem is proven.

REFERENCES

1. R. H. Dicke, "The Measurement of Thermal Radiation at Microwave Frequencies," *Rev. of Sci. Instr.*, Vol. 17, 1946, p. 268.
2. G. L. Abbas and V. W. S. Chan, "Optimal Design and Performance of a Dual-Detector Optical Heterodyne Receiver for Local Oscillator Noise Suppression," *I.E.E.E. Global Telecomm. Conf. Record*, San Diego, CA, November 1983, p. 422.
3. T. K. Yee, "Intensity Noise of GaAlAs Laser Diodes at Various Output Powers and Frequencies," *Conf. on Lasers and Electro-Optics Technical Digest*, Baltimore, MD, May 1983, p. 46.
4. H. Jackel and H. Melchior, "Fundamental Limits of the Light Intensity Fluctuations of Semiconductor Lasers with Dielectric Transverse Mode Confinement," *Optical Comm. Conf.*, Amsterdam, The Netherlands, 1979 p. 2.5-1.
5. B. M. Oliver, "Signal-to-Noise Ratios in Photoelectric Mixing," *Proc. I.R.E.*, Vol. 49, 1961, p. 1960.
6. H. A. Haus and C. H. Townes, "Comments on 'Noise in Photoelectric Mixing,'" *Proc. I.R.E.*, Vol. 50, 1962, p. 1544.
7. T. Waite and R. A. Gudmundsen, "A Balanced Mixer for Optical Heterodyning: The ANN Detector," *Proc. I.E.E.E.*, Vol. 54, 1966, p. 297.
8. T. Waite, "A Balanced Mixer for Optical Heterodyning: The Magic T Optical Mixer," *Proc. I.E.E.E.*, Vol. 54, 1966, p. 334.
9. H. van de Stadt, "Heterodyne Detection at a Wavelength of $3.39\ \mu\text{m}$ for Astronomical Purposes," *Astron. and Astrophys.*, Vol. 36, 1974, p. 341.
10. H. P. Yuen and V. W. S. Chan, "Noise in Homodyne and Heterodyne Detection," *Opt. Lett.*, Vol. 8, 1983, p. 177.
11. G. L. Abbas, V. W. S. Chan, and T. K. Yee, "Local-Oscillator Excess-Noise Suppression for Homodyne and Heterodyne Detection," *Opt. Lett.*, Vol. 8, 1983, p. 419.
12. T. K. Yee, G. L. Abbas, and V. W. S. Chan, "Study of Intensity Noise Statistics and Power Spectra of GaAlAs Laser Diodes at Various Output Powers and Frequencies," to be published.
13. T. L. Paoli and J. E. Ripper, "Observation of Intrinsic Quantum Fluctuations in Semiconductor Lasers," *Phys. Rev. A*, Vol. 2, 1970, p. 2551.

14. S. K. Sheem and T. G. Giallorenzi, "Single-Mode Fiber-Optical Power Divider: Encapsulated Etching Technique," *Opt. Lett.*, Vol. 4, 1979, p. 29.
15. C. L. Chen and W. K. Burns, "Polarization Characteristics of Single-Mode Fiber Couplers," *I.E.E.E. Journ. of Quant. Electr.*, Vol. QE-18, 1982, p. 1589.
16. D. Gloge, P. W. Smith, D. L. Bisbee, and E. L. Chinnock, "Optical Fiber End Preparation for Low-Loss Splices," *Bell System Tech. Journ.*, Vol. 52., 1973, p. 1579.
17. G. L. Abbas, V. W. S. Chan, and T. K. Yee, "Cancellation of Local-Oscillator Intensity Noise Due to the Relaxation Oscillation of GaAlAs Lasers with a Dual-Detector Heterodyne Receiver," *Conf. on Opt. Fiber Comm.*, New Orleans, LA, January 1984.
18. T. K. Yee, V. W. S. Chan, and G. L. Abbas, "Intensity Noise Statistics of GaAlAs lasers," *Conf. on Opt. Fiber Comm.*, New Orleans, LA, February 1983.
19. R. S. Kennedy, "Communication Through Optical Scattering Channels: An Introduction," *Proc. I.E.E.E.*, Vol. 58, 1970, p. 1651.